EPIGENOMICS
2026, VOL. 18, NO. 1, 27–44
https://doi.org/10.1080/17501911.2025.2603883

Taylor & Francis
Taylor & Francis Group

RESEARCH ARTICLE

Mitochondrial DNA copy number reduction via *in vitro TFAM* knockout remodels the nuclear epigenome and transcriptome

Phyo W. Win[a], Julia Nguyen[a], Elly H. Shin[a], Tyler S. Nagano[a], Brent Selimi[a], Katie Hong[b], Anahita M. Meybodi[a], Bradley P. Yates[b], Emma V. Burke[b], David E. Carter[c], Gregory A. Newby[b,d,e,f], Charles Newcomb[b], Dan E. Arking[b] and Christina A. Castellani[a,b,g,h]

[a]Department of Pathology and Laboratory Medicine, Schulich School of Medicine and Dentistry, Western University, London, Ontario, Canada; [b]McKusick-Nathans Institute, Department of Genetic Medicine, Johns Hopkins University School of Medicine, Baltimore, MD, USA; [c]London Regional Genomics Centre, Robarts Research Institute, London, Ontario, Canada; [d]Department of Biomedical Engineering, Johns Hopkins University, Baltimore, MD, USA; [e]Institute for Nanobiotechnology, Johns Hopkins University, Baltimore, MD, USA; [f]Department of Molecular Biology and Genetics, Johns Hopkins University, Baltimore, MD, USA; [g]Department of Epidemiology and Biostatistics, Schulich School of Medicine and Dentistry, Western University, London, Ontario, Canada; [h]Children's Health Research Institute, Lawson Research Institute, London, Ontario, Canada

ABSTRACT

Aims: Mitochondrial DNA copy number (mtDNA-CN) is associated with several age-related chronic diseases and is a predictor of all-cause mortality. Here, we examine site-specific differential nuclear DNA (nDNA) methylation and differential gene expression resulting from in vitro reduction of mtDNA-CN to uncover shared genes and biological pathways mediating the effect of mtDNA-CN on disease.

Materials and methods: Epigenome and transcriptome profiles were generated for three independent human embryonic kidney (HEK293T) cell lines harboring a mitochondrial transcription factor A (TFAM) knockout generated via CRISPR-Cas9, and matched control lines.

Results: We identified 2924 differentially methylated sites, 67 differentially methylated regions, and 102 differentially expressed genes associated with mtDNA-CN. Integrated analysis uncovered 24 Gene-CpG pairs. $GABA_A$ receptor genes and related pathways, the neuroactive ligand signaling pathway, ABCD1/2 gene activity, and cell signaling processes were overrepresented, providing insight into the underlying biological mechanisms facilitating these associations. We also report evidence implicating chromatin state regulatory mechanisms as modulators of mtDNA-CN effect on gene expression.

Conclusions: We demonstrate that mitochondrial DNA variation signals to the nuclear DNA epigenome and transcriptome and may lead to nuclear remodeling relevant to development, aging, and complex disease.

PLAIN LANGUAGE SUMMARY

The amount of mitochondrial DNA, called mitochondrial DNA copy number (mtDNA-CN), has been linked with risk for various health conditions and diseases. To better understand this relationship, we studied the association between mtDNA-CN reduction and other DNA changes within the cell, specifically those in the cell nucleus. Using a cell model, we compared changes in cells with lower mtDNA-CN to normal cells. We noticed several patterns of changes that point to different genomic regions, communication processes, and signaling pathways within the cells that may be involved in the association of mtDNA-CN with disease development. Our findings help explain how the mitochondria interact with the nucleus in the context of complex disease.

ARTICLE HISTORY
Received 16 October 2024
Accepted 10 December 2025

KEYWORDS
Mitochondria; mitochondrial DNA; epigenome; transcriptome; mitochondrial DNA copy number

1. Introduction

Mitochondria are cytoplasmic organelles that are essential to cell metabolism. They are central to many cellular functions such as oxidative phosphorylation, apoptotic processes, and cell differentiation via cell signaling [1]. Despite widespread evidence that mitochondrial DNA (mtDNA) mutations affect many diseases, the biological mechanisms responsible for mitochondrial dysfunction leading to age-related diseases are largely unknown. Unlike nuclear DNA (nDNA), which is present in two copies per cell, mitochondria have multiple copies of mtDNA per cell (100s to 1000s). The exact number of mtDNA per cell is highly variable depending on cell type and declines with age [2]. Reductions in mitochondrial DNA copy number (mtDNA-CN) have been associated with reduced respiratory enzyme activity, lower expression of proteins in oxidative phosphorylation, and differences in cellular characteristics [3]. mtDNA-CN variation has been associated with many age-related diseases such as cardiovascular disease [4–7], kidney-related diseases [8,9], respiratory diseases [10,11], obesity [12], cancers [13–16], neurodegenerative diseases [17],

CONTACT Christina A. Castellani christina.castellani@schulich.uwo.ca Department of Pathology and Laboratory Medicine, Schulich School of Medicine and Dentistry, Western University, Room 4011, Dental Sciences Building, 1151 Richmond St, London, ON N6A 3K7, Canada

Supplemental data for this article can be accessed online at https://doi.org/10.1080/17501911.2025.2603883

Article highlights

- Mitochondrial DNA copy number (mtDNA-CN) is associated with several age-related diseases.
- Knockout of mitochondrial transcription factor A (TFAM) results in a stable reduction of mtDNA-CN in cell models.
- 2,924 differentially methylated sites, 67 differentially methylated regions, 102 differentially expressed genes, and 24 Gene-CpG pairs associated with mtDNA-CN were identified.
- $GABA_A$ receptor genes and related pathways, the neuroactive ligand signaling pathway, ABCD1/2 gene activity, and cell signaling processes were overrepresented.
- Overall, we demonstrate that mtDNA variation signals to the nuclear epigenome and transcriptome, leading to nuclear remodeling that may be relevant to development, aging, and complex disease.

and diabetes [18], and reduced mtDNA-CN has been associated with all-cause mortality [19]. mtDNA-CN estimates are readily obtained using DNA from blood samples, hence may serve as a potential clinically relevant biomarker of mitochondrial function and disease risk.

The nuclear epigenome consists of a collection of chemical modifications to DNA and associated proteins that may dynamically influence gene and phenotypic expressions in response to changes in the internal and external environment. DNA methylation, the most well-understood epigenetic mark, involves the addition of a methyl group to cytosine residues adjacent to guanine residues; these CG dinucleotides are called CpG sites [20]. Promoters are often located within close proximity to clusters of CpGs such that the methylation status of these CpG islands can affect gene expression by preventing interactions with transcriptional machinery [21]. Typically, transcription factors are unable to bind promoters that are heavily methylated, hence the gene cannot be transcribed [21].

Bi-directional communication between mtDNA and nDNA is essential for maintaining homeostasis, normal cell functioning, and the structural integrity of the cell [22,23]. A pioneering study reported that depletions in mtDNA levels have significant effects on nDNA methylation patterns that may contribute to tumorigenesis [24]. This initial discovery has since been supported by multiple studies that have demonstrated the link between mitochondrial DNA variation and the nuclear epigenome. Studies have identified significant associations between mtDNA-CN, CpG methylation, and gene expression in human cohorts, and *in vitro* models [25–28]. Associations between mtDNA sequence variation and the nuclear epigenome have also been observed [29–32]. Despite these associations, the mechanisms driving the relationship of mtDNA modification to the nuclear epigenome and transcriptome remain unknown.

Mitochondrial transcription factor A (*TFAM*) is a nuclear-encoded mtDNA binding protein with an essential role in mitochondrial transcription initiation and mtDNA-CN regulation, such that mtDNA-CN measures are positively correlated with TFAM protein level [33,34]. *TFAM* knockout (KO) has demonstrated a reduction in mtDNA-CN *in vitro* [35], with several studies reporting resulting mitochondrial dysfunction [36–39]. The reduction of *TFAM* gene expression in cells lead to decreased mtDNA-CN and disrupted mitochondrial function, suggested by mitochondrial swelling, leakage of mtDNA to the cytoplasm, lower oxygen consumption rates, and increased production of reactive oxygen species (ROS) [39]. Additionally, long-term *TFAM* loss affects ROS production and mitochondrial oxidation leading to decreased oxygen consumption and ATP concentration [40]. Knockout of the *TFAM* gene has been shown to reduce mtDNA-CN *in vivo* as well, shown by heterozygous *TFAM* knockout mouse models displaying reduced mitochondrial transcription and oxidative phosphorylation [35]. Further, a clinical report on two siblings with *TFAM* deficiency identified mtDNA depletion in liver and skeletal muscles, along with reduced mitochondrial basal respiration and spare respiratory capacity [41]. Metabolites such as S-adenosylmethionine (SAM) and acetyl-CoA, which are influenced by mitochondrial function, serve as key mediators in the epigenetic regulation of nDNA, potentially linking mtDNA-CN change to altered nuclear epigenome and transcriptome profiles [42–44]. Studies have also revealed *TFAM* knockout to influence nDNA methylation and/or gene expression in mice [45,46]. Previous studies have also shown that mtDNA-CN reduction leads to widespread methylation changes in non-coding regions, including enhancers and intergenic open seas, rather than only promoters or CpG islands [47–49]. Conversely, methylation changes at promoter CpG islands can directly alter transcription factor binding and gene expression [21]. Therefore, examining the distribution of methylation changes across different genomic regions, alongside gene ontology enrichment, could provide further insight into how TFAM KO and mtDNA-CN reduction could be remodeling the nuclear regulatory system. We have used our *TFAM* knockout model to interrogate the effect of mtDNA on nDNA methylation and gene expression at specific CpGs/genes identified in an epigenome-wide association study (EWAS) of mtDNA-CN [25].

To further characterize the underlying biological mechanisms that drive the global effect of *TFAM*-induced mtDNA-CN variation on nDNA methylation, we use our *TFAM* knockout cell line model to observe the effects of *in vitro* reduction of mtDNA-CN on the global nuclear epigenome and transcriptome profiles. For our current study, we hypothesize that *TFAM* KO-induced reduction in mtDNA-CN alters the nuclear epigenetic and gene expression profiles through disruption in mitochondrial metabolites and signaling pathways, such as those implicated in mitochondrial-nuclear crosstalk. Through the integration of differentially methylated and differentially expressed genes, our results provide insight into the biological mechanisms which mediate the effect of mtDNA-CN on aging-related diseases.

2. Materials and methods

2.1. TFAM knockout cell line model

The experimental models generated in this study were modified human embryonic kidney (HEK293T) cell lines with a knockout of the *TFAM* generated via CRISPR-Cas9 using the Origene *TFAM* – Human Gene Knockout Kit following the manufacturer's protocol (*TFAM* KO). The sgRNA guide sequence used was GCGTTTCTCCGAAGCATGTG. Turbofectin 8.0 was used to perform lipofection, and puromycin was

used for selection. The sgRNA guide sequence for the CRISPR-Cas9 knockout of *TFAM* (ENSG00000108064) was designed to target chromosome 10 (S1 Fig). The knockout procedure was performed independently for each of the three KO cell lines. Three negative control (NC) cell lines were generated using the same original cell line performing all identical steps but without performing the knockout. This resulted in 6 independent samples (3 KO and 3 NC). The sequencing primers used to confirm the *TFAM* knockout are as follows: *TFAM*_Left_Forward_Primer_2: AGCGACTGTGGACAACTAGC, GFP_Reverse_Primer_2: TCATCTTGTTGGTCATGCGG, Puro-Forward_Primer_1: CACAACCTCCCCTTCTACGAG, *TFAM*_Right _Reverse_Primer_1: CCCCAAACTCCTTACCTGGG.

2.1.1. CRISPR off-target analysis

CRISPR-Cas9 off-target effects on the *TFAM* KO samples were determined through the assessment of predicted off-target regions of interest using Integrated DNA Technologies (IDT) sgRNA checker for CRISPR-Cas9 guide RNA (GCGTTTCTCCGAACGCATGTG), which was used to generate *TFAM* KO lines. Each target region's off-target risk score was provided as a score from 0–100. Three regions with the lowest off-target risk scores, indicating the highest predicted possible off-target edits, and six regions with an overlapping gene, as well as *TFAM* (positive control), were chosen as regions of interest (S12 Table). All target regions were assessed in three independent *TFAM* KO lines (KO5, KO6, KO11) and three negative control lines (NC1, NC2, NC3). Primer pairs were designed using Primer3 and PrimerBLAST for each target region. Genomic DNA from the three *TFAM* KO and negative control lines were used for the initial PCR amplification. This first-round of PCR was performed to amplify the candidate off-target regions in each sample and to attach adaptor sequences, followed by another PCR amplification performed to attach the Illumina MiSeq index primers to the adhered adaptor sequences, following the protocol provided in Huang et al. [50]. Each sample was provided a unique forward index primer, and each target was provided a unique reverse index primer to produce unique index combinations per sample per target. The PCR cycling protocol followed that provided by Huang et al., and all PCR products were assessed using 1% agarose gel electrophoresis with ethidium bromide staining. Once confirmed, all samples per target were quantified using the Qubit 2.0 Fluorimeter dsDNA High Sensitivity Assay Kit (Thermo Fisher Scientific, Waltham, MA) and pooled based on the molar concentration of the amplicons. Each target pool underwent gel electrophoresis followed by excision of the band of interest using QIAquick Gel Extraction Kit.

For off-target analyses, all samples were sequenced at the London Regional Genomics Centre (Robarts Research Institute, London, Ontario, Canada) or at Johns Hopkins University Department of Genetic Medicine using the Illumina MiSeq (Illumina Inc., San Diego, CA). The specific target pools were quantified using the Qubit 2.0 Fluorimeter dsDNA High Sensitivity Assay Kit (Thermo Fisher Scientific, Waltham, MA) and further pooled using molar concentration. Final pooled library size was assessed on the Agilent 4150 TapeStation using the High Sensitivity D1000 Reagents (Agilent Technologies Inc., Palo Alto, CA) and quantified using the Qubit. The library was sequenced on an Illumina MiSeq as a 1×301 bp single end run, using a Micro Kit v2 at a concentration of 11 pM. The sequenced fastq files were analyzed using CRISPResso2 [51]. Files for each amplicon were analyzed using CRISPRessoBatch, with q score threshold of 30 and analysis window size of 20. To avoid double-counts of insertion and deletion (indel) events, indel frequencies were calculated as the sum of reads with only insertions, only deletions, and any combination of insertion and/or deletion with each other or with substitutions, divided by the number of aligned reads.

We observed poor alignment (<20 aligning reads) for three amplicons including the target TFAM locus, the off-target on Chr6, and the off-target on Chr13. New primers were designed for these loci by hand to avoid repetitive elements. New PCR amplicons were amplified, pooled, and gel-purified on a 1% agarose gel. New amplicons were sequenced using a 300 cycle single end run on a MiSeq using a standard v2 kit at a concentration of 10 pM. Fastq files were aligned by CRISPResso with standard parameters including a q score cut-off of 30. While this was sufficient to identify and align sample reads for all off-target sites including those sequenced alongside the new TFAM on-target amplicon, the on-target TFAM amplicon itself yielded lower q-scores, which we attribute to likely be caused by the particularly A/T-rich sequence context. Greater than 95% of reads aligned using CRISPResso2 when a q score threshold of 2 was used for the TFAM target, so this adjusted parameter was used for TFAM analysis only.

A t-test was used to determine statistical significance of any difference in indel frequencies calculated by CRISPResso2 between treated *TFAM* KO and NC lines. Visual inspection of the nucleotide frequency plots generated by CRISPResso2 revealed no characteristic Cas9-induced indel patterns at any of the candidate off-target sites.

2.1.2. Karyotype Analysis

Metaphase chromosome preparations were performed according to standard cytogenetic protocols. Briefly, cells were harvested during logarithmic growth phase following treatment with colcemid (0.1 µg/mL) for 1–2 hours to arrest cells in metaphase. After hypotonic treatment with 0.075 M KCl at 37°C for 15–20 minutes, cells were fixed in freshly prepared methanol:acetic acid (3:1) fixative through multiple changes. Fixed cells were dropped onto clean glass slides and air-dried. G-banding was performed using trypsin treatment followed by Giemsa staining. A minimum of 20 metaphases were analyzed per sample using a fully automated karyotyping system, and karyotypes were described according to the International System for Human Cytogenomic Nomenclature (ISCN, 2024). Clonal abnormalities were confirmed and documented if present in at least two independent cultures.

2.2. Mitochondrial DNA copy number quantification

mtDNA-CN was quantified using a multiplexed qPCR assay with ABI TaqMan chemistry (Applied Biosystems). Each reaction consisted of 20 ng of genomic DNA, with a primer-limited

assay targeting the mitochondrial *ND1* gene (Assay ID Hs02596873_s1) and a nuclear *RPPH1* gene (Assay ID Hs03297761_s1) [19]. Each independent sample was run in a minimum of technical triplicates using an ABI Viia7 system. Cycle threshold (Ct) values were determined using ABI Viia7 software. The delta Ct value was calculated as delta Ct = *RPPH1* Ct – *ND1* Ct.

2.3. TFAM overexpression

A *TFAM* overexpression plasmid (Addgene #129573) was used to reintroduce *TFAM* into the *TFAM* KO and NC lines. *TFAM* KO and NC cells were plated and left to adhere for 24 hours before transfection. Cells were given the overexpression plasmid through lipofection with Lipofectamine LTX (Invitrogen #15338100) as per the manufacturer's protocols. Negative control samples received a transfection cocktail also containing Lipofectamine LTX but without the *TFAM* overexpression plasmid. Cells were grown for 48 hours before RNA and DNA isolations.

RNA was isolated following the manufacturer's protocol for the RNeasy Plus Mini Kit (Qiagen 74,134) while DNA was isolated with phenol:chloroform:isoamyl alcohol. Both RNA and DNA underwent an ethanol precipitation clean-up before further downstream processing. Sample quality and concentrations were assessed using a Nanodrop 1000 for both DNA and RNA, and DNA samples were further quantified with the Qubit 1x dsDNA BR Assay (Invitrogen #Q33266) and Qubit 4.0 system and diluted to 10–20 ng/µL using molecular-grade water. Contaminating genomic DNA was first removed from the RNA samples. Approximately 1 µg of purified RNA from each sample was then converted into complementary DNA (cDNA) using the SuperScript IV with ezDNase kit (Invitrogen #18091150) by following the manufacturer's protocol. Genomic DNA was first removed with the provided ezDNase enzyme, and the cDNA was synthesized using random hexamers. Upon completion of the protocol, the resulting cDNA was then quantified using the Qubit ssDNA Assay (Invitrogen #Q10212) on the Qubit 4.0 system and diluted to 10 ng/µL using molecular-grade water.

Gene expression differences after overexpression were performed using various 20x Taqman qPCR gene expression assays, including assays for the *TFAM* gene and eight additional significantly differentially expressed genes identified to be differentially expressed by *TFAM* KO analysis. The gene expression assays were performed using the Taqman gene expression master mix (ThermoFisher #4369016) and *HPRT1* (Assay ID Hs02800695_m1) housekeeping gene. The specific assays used were *TFAM* (Assay ID Hs00273372_s1), *CA2* FAM (Assay ID Hs01070108_m1), *CA8* (Assay ID Hs01015824_m1), *FLRT2* (Assay ID Hs00544171_s1), *SFRP2* (Assay ID Hs01564480_m1), *SLC16A2* (Assay ID Hs00185140_m1), *RPLL22L1* (Assay ID Hs01595626_g1), *DSEL* (Assay ID Hs00707488_s1), and *ABCD1* (Assay ID Hs00163610_m1). The *HPRT1* housekeeping gene chosen used the VIC-MGB dye, while all other assays used the FAM-MGB dye. Ct values were filtered to exclude failed amplifications, high standard deviation replicates, or non-amplified samples. The delta Ct values were calculated for each target gene by subtracting the Ct value of the *HPRT1* reference gene. Replicates with a high coefficient of variation were removed. Significant change in expression was determined by one-tail t-test.

2.4. DNA/RNA data generation for methylation and RNA-sequencing analysis

DNA was extracted using the AllPrep DNA/RNA Mini Kit following manufacturer's protocol and quantified using a Nanodrop 1000. Bisulfite conversion of 1 µg genomic DNA was performed using the EZ-96 DNA Methylation Kit (Deep Well Format) (Zymo Research D5004; Irvine, CA, USA) according to the manufacturer's protocol. Bisulfite conversion efficiency was determined by PCR amplification of the converted DNA using Zymo Research's Universal Methylated Human DNA Standard and Control Primers. Following bisulfite conversion, DNA strands were hybridized to the Illumina Infinium EPIC BeadChip to determine the DNA methylation profile for over 850,000 CpGs in the human genome. All samples (3 KO and 3 NC) were run on the EPIC BeadChip at two separate time points which resulted in 12 individual runs represented by 12 raw.idat files (6 KO and 6 NC). DNA, RNA, and protein isolation was performed on samples collected at passages 32, 37, and 45. qPCR for mtDNA-CN measurement was conducted using the same DNA isolations. EPIC arrays were performed on DNA from passage 32 and 37.

RNA extraction, quantification, quality control, library preparation, and sequencing were performed using the Qiagen AllPrep DNA/RNA Mini Kit, Qubit 2.0 Fluorometer, and Illumina's TruSeq Stranded Total RNA kit. Total RNA from passage 45 was converted to cDNA, and end repair was performed. Fragments were ligated and size selected. The Illumina HiSeq 2500 instrument was used to perform paired-end 150 bp sequencing to generate gene expression profiles. Each of the 6 samples (3 KO and 3 NC) were sequenced twice which resulted in 12 FASTQ files.

2.5. nDNA methylation analysis of cell lines

The minfi package was used for EPIC BeadChip analysis and quality control to remove poor quality probes [52]. The data was normalized using functional normalization [53] and poor quality probes were removed if the probe had a detection p-value > 0.01. Cross-reactive probes were identified and omitted [54], as well as probes with known SNPs at the CpG site. As each sample was run in technical replicates, to ensure that the observed methylation differences were attributable to *TFAM* KO rather than technical variability, we filtered out CpG sites where the mean methylation beta value between the first and second technical runs for control lines differed by more than 0.15. NC lines were chosen for this QC step due to the expectation that their values would represent a stable metric for comparison.

Differentially methylated sites were determined using a linear model with mtDNA-CN as the independent variable and methylation *M* values as the dependent variable using both DMPFinder in minfi and a linear mixed model [52]. We initially conducted a principal component analysis on

methylation beta values to assess other unaccounted confounders, finding PC1 correlated with mtDNA-CN ($r = 0.96$, $p < 7.17E-7$) and PC5 with Batch ($r = 0.73$, $p = 0.007$) (S3 Fig), and added surrogate variables 1 and 2 to our linear mixed model to capture unaccounted variation while preserving mtDNA-CN signals. The chosen linear mixed model incorporated sample ID as a random effect to account for sample duplicates, as well as methylation batch (1st and 2nd run), and the first two surrogate variables (SV) as fixed effects. A significance threshold of FDR < 0.05 was used to determine differentially methylated sites.

Differentially methylated regions (DMRs) were determined via linear modeling using the R package DMRcate with treatment status (KO vs NC) as the independent variable and methylation *M* value as the dependent variable [55]. Following our approach for differentially methylated sites, sample ID was incorporated as a random effect along with batch, SV1, and SV2 as fixed effects for DMR calling. A significance threshold of FDR < 0.05 was used to determine differentially methylated sites prior to DMR identification. Regions were defined as having a minimum of 10 CpGs with at most 1000 bps between CpGs within the region. Additionally, regions were removed if the region had a mean beta value difference < 0.20 between KO and NC. A significance threshold of FDR < 0.05 was used to identify significant DMRs.

2.6. RNA-Sequencing analysis of cell lines

Kallisto was used to pseudo-align the compressed FASTQ files to the Genome Reference Consortium Human Build 37 to generate transcript level counts [56]. To account for uncertainties in transcript counts, a total of 100 bootstraps were performed in Kallisto. Transcript level counts were converted to gene level counts using the transcript count of the isoform with the highest expression.

Normalization, quality control, and differential expression analysis were performed using the EdgeR package [57]. Genes with less than 20 reads across all samples were removed due to low expression. The data was normalized to scale for effective library size of samples using the trimmed mean of M-values (TMM) [58]. Gene expression was modeled using a weighted likelihood empirical Bayes method as described by Chen et al. [59]. Differentially expressed genes were determined using a likelihood ratio test between the null and the observed mode, adjusting for sample ID, batch, SV1 and SV2. Genes with an absolute log fold-change <2 were removed. A significance threshold of FDR < 0.05 was used to determine differentially expressed genes.

2.7. Integration of methylation and gene expression

The ELMERv2 [60] package was used to integrate differential methylation and differential gene expression to find associations between methylation and gene expression of nearby genes. Associations with any direction of effect were considered. The supervised approach was used such that methylated and unmethylated groups were split into KO and NC labels. All CpGs and genes were used as the methylation and the gene expression data inputs respectively.

Each CpG site was mapped to the nearest 20 genes (10 upstream and 10 downstream) within 1Mbp. Following the same parameters to previous studies, Gene-CpG pairs were removed from the analysis if the CpG was greater than 1 Mbp from the transcriptional start site of the gene using the ENSEMBL [61] gene-level annotations [25,62]. To capture proximal CpG–gene interactions and to identify regulatory relationships, pairs containing both significantly differentially methylated CpGs and significantly differentially expressed genes were prioritized for further analysis. A significance threshold of false discovery rate (FDR) < 0.05 was used to determine significant Gene-CpG pairs.

2.8. Enrichment analyses

Enrichment analyses were performed on the differential methylation sites/regions and differential gene expression results with all tested sites, regions, or genes as background, respectively. We leveraged the following databases to uncover physiological mechanisms overrepresented in our results: The Gene Ontology (GO) [63,64] database for functional gene groups, the Kyoto Encyclopedia of Genes and Genomes (KEGG) [65–67] for biological pathways, the Reactome Pathway and transcription factor gene sets from the Molecular Signatures Database (MSigDB) [68,69], and the MitoCarta3.0 [70] database for mitochondrial related genes and pathways.

GO and KEGG over-enrichment analysis were performed on the significant methylation sites and methylation region results using missMethyl [71]. missMethyl is particularly well suited for this as it accounts for the bias introduced from unbalanced CpG-gene mapping. GO and KEGG functional enrichment analyses were performed on significant genes from RNA-sequencing using limma [72]. The top KEGG pathways were visualized using Pathview to map up/down-regulation of genes within pathways [73]. Reactome pathway functional enrichment [74] was performed on differentially methylated sites using the MethylGSA package [75] using FDR < 0.05 and differentially expressed genes using the ReactomePA package [76].

MSigDB transcription factor binding sites, regulatory target gene sets, and MitoCarta3.0 mammalian mitochondrial protein sets and pathways were used to perform over-enrichment analysis on significant methylation and gene expression results. Overrepresentation of transcription factor genes was determined by using the Student's t-test on significant genes in the gene set against the genes that were not present in the gene set. A significance threshold of p-value < 0.05 was used. In addition, the significant genes from the RNA analysis were tested for overlaps with genes in MitoCarta3.0 using a Chi-squared test ($p < 0.05$).

For the GO, KEGG, and transcription factor enrichments, the methylation and gene expression results were combined using the Fisher's combined probability test to combine p-values [77]. Fisher's combined probability test could not be applied to Reactome results due to the lack of methylation results

following p-value filtering. The methylation site and the methylation region results were combined separately with the gene expression results using this method. Terms/groups with p-value > 0.05 in either the methylation or gene expression results were removed before combining p-values.

The EWAS Catalog was used to identify any differentially methylated CpG sites that have been previously reported in the literature to be associated with known phenotypes. CpG sites and their associated phenotypic traits were obtained from the EWAS Catalog website in June 2023. Traits were further collapsed into broader disease categories. We applied a pruning method to select the most significant CpG site per 1 Mbp window from the 2924 significantly differentially methylated probes (FDR < 0.05) identified in the EWAS. Specifically, CpG sites were annotated, and sorted by chromosome and position. For each chromosome, we iterated through the CpG sites, retaining the CpG with the lowest p-value within each 1 Mbp window, which resulted in 1029 unique CpGs after pruning. This approach mitigated the influence of correlated methylation signals from closely spaced CpGs. To assess for enrichment in overlapping CpGs with given specific disease terms, 1029 CpGs were randomly selected from the EWAS Catalog (representing the total number of pruned CpGs from our *TFAM* knockout differently methylated probes). Further, the overlap between the randomized set and each disease category was recorded. This was repeated for 1000 permutations with the p-value measured as the percentage of the number of permutations in which the number of overlapping CpGs was greater than the observed number of overlapping CpGs.

Enrichment of genomic regions was performed using the DMRichR [78] package to test for overrepresented CpG categories (CpG islands, shores, shelves, and open sea) and gene regions (promoter, UTR, exon, intron, downstream, intergenic, active TSS, transcription, enhancers, ZNF genes and repeats, heterochromatin, PolyComb, quiescent/low). The enrichment testing for overrepresented CpG and gene regions used a Fisher's Exact test at a significance threshold of FDR < 0.05. The DMRichR package also includes a wrapper for LOLA [79] which tests for enrichment of 15 chromatin states from ChromHMM [80]. Enrichment testing for chromatin states used a Fisher's Exact test, and a significance threshold of FDR < 0.05 was used.

3. Results

3.1. TFAM knockout reduces mtDNA-CN and TFAM expression in a cell model

For this report, we used lines generated from our earlier published work (Castellani et al., 2020), where knockout (KO) of mitochondrial *TFAM* in HEK293T cells was performed via CRISPR-Cas9 generating three independent *TFAM* KO lines and three corresponding negative control lines. Sanger sequencing confirmed disruption of *TFAM* in all three independent knockout lines, which was further assessed by qPCR of *TFAM* DNA using a primer that overlaps with the cleavage site confirming loss of the *TFAM* gene (as described in Castellani et al., 2020) [25]. mtDNA-CN was found to be consistent across passages and was significantly reduced in the *TFAM* KO lines compared to the NC lines ($p < 2.2E\text{-}16$, S2 Fig, S13 Table). *TFAM* gene expression was also measured using qPCR (S11 Table). Gene expression was determined using the double delta cycle threshold (Ct) method. The *TFAM* knockout efficacy was previously described and exhibited a 5-fold reduction in *TFAM* mRNA expression and an 81% decrease in protein levels as confirmed by qPCR and western blot (Figure 4, Castellani et al. (2020)) [25]. *TFAM* KO lines demonstrated a 18-fold reduction in mtDNA-CN compared to negative control lines (Figure 4 in Castellani et al, 2020) [25]. We note that this reduction reflects total mtDNA-CN, as measured by qPCR, and does not assess the total number of mitochondria.

In this current report, we further assess the three independent *TFAM* KO and three matched NC lines generated from the same parental HEK293T cells with respect to karyotypic stability, mtDNA-CN maintenance across passages, and CRISPR off-target effects. Karyotyping analysis via a minimum of 20 metaphases per sample using an automated karyotyping system, revealed a stable consensus karyotype of 64–68 < 3n > XX across all six lines (NC and *TFAM* KO), confirming chromosomal stability. To assess stability of mtDNA-CN levels across passage number, we quantified mtDNA-CN in technical triplicates across cell passages 32, 37, and 45. *TFAM* KO lines exhibited a consistent reduction in mtDNA-CN, as compared to NC lines, across all tested passages (p-value < 2.2E-16), confirming stable mtDNA-CN depletion for *TFAM* KO lines (S2 Fig, S13 Table). We further assessed the potential for off-target editing in two ways. First, editing via *in silico* CRISPR off-target analysis which prediction using the IDT sgRNA design tool, assigned the chosen guide RNA to have predicted low off-target activity. Secondly, nine candidate predicted off-target loci with the highest predicted off-target score from *in silico* analysis, plus the on-target *TFAM* locus were tested via targeted Illumina sequencing to assess gene disruption (S12 Table). CRISPResso2 analysis of the targeted Illumina sequencing revealed over 90% disruption of the target *TFAM* gene in the *TFAM* KO lines. In contrast, no off-target edits were identified (S12 Table).

3.2. Site-specific nuclear methylation differences are associated with TFAM knockout

An EWAS using 3 *TFAM* KO cell lines and 3 normal control (NC) cell lines (all samples were run in technical duplicates) was conducted to identify site-specific differential methylation. Following normalization and quality control, 769,026 CpG sites were assessed for differential methylation between NC and KO lines. Our linear model identified 2924 CpGs to be differentially methylated following *TFAM* KO and subsequent reduction of mtDNA-CN (FDR < 0.05) (Figure 1(A,B), S1 Table). The quantile-quantile plot (S4A Fig) and lambda value (lambda = 3.39) showed high inflation. To assess if the inflation was due to true signal or technical artifacts, we ran 500 null permutation tests which indicated that the signal was robust and representing true signal (S4B Fig). Additionally, no chromosomal bias was identified. No overlap was found between our differently methylated sites and known phenotypes from the EWAS catalog after pruning and look up using the EWAS catalog's disease categorization.

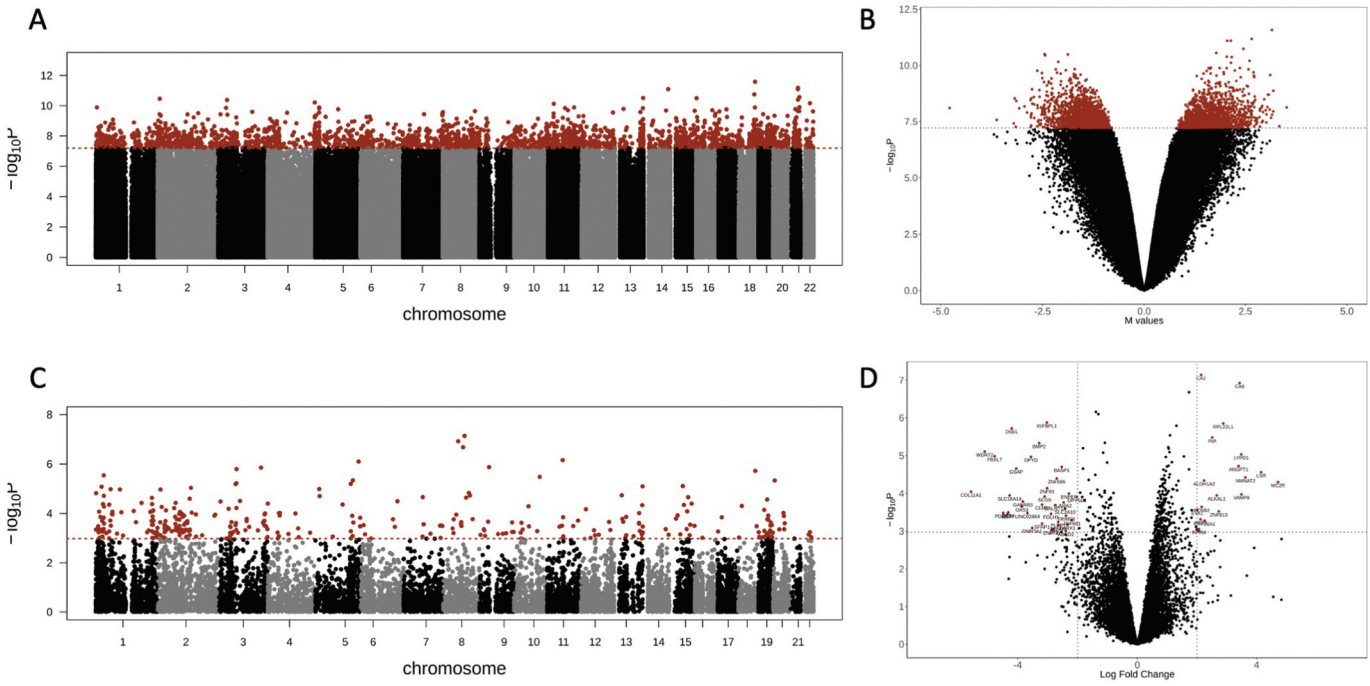

Figure 1. Results from differential methylation and gene expression analysis. (A) Manhattan plot of methylation sites across the genome. Red data points correspond to differentially methylated sites (FDR < 0.05). (B) Volcano plot of methylation *p*-values and effect sizes. Red data points correspond to differentially methylated sites (FDR < 0.05). (C) Manhattan plot of gene transcripts across the genome. Red data points correspond to differentially expressed genes (FDR < 0.05). (D) Volcano plot of gene expression *p*-values and effect sizes. Red data points correspond to differentially methylated sites (FDR < 0.05).

3.3. *TFAM* knockout lines exhibit region-level nuclear methylation changes

Differential methylated region (DMR) analysis was performed to identify clusters of CpGs in the same region that were differentially methylated in *TFAM* KO lines. DMRs identified by Fisher's combined probability transform (DMRcate) identified 102 regions were differentially methylated (FDR < 0.05) between *TFAM* KO and NC cells (S2 Table). Seventy-five regions (74.0%) were hypomethylated in the KO group while 27 regions (26.0%) were hypermethylated in the KO group indicating reduced global methylation levels in the *TFAM* KO group compared to the NC group (S2 Table) (*p*-value = 0.0009 for hypomethylation bias). Biological replicates (2 per independent cell line) showed consistent methylation patterns, as demonstrated by four representative plot examples (Figure 2(A–D)) and supported by underlying individual-level data (S2 Table).

3.4. *TFAM* knockout leads to differential nuclear gene expression

RNA sequencing was performed to evaluate differential gene expression between our *TFAM* KO and NC cell lines, with each independent cell line analyzed in duplicate and adjusted for batch. After normalization and quality control steps were performed, 14,781 genes remained to test for differential gene expression. Sixty-seven genes were differentially expressed (FDR < 0.05 and absolute log fold change >2) with no chromosomal bias identified (Figure 1(C,D), S3 Table). A bias between upregulation and downregulation of gene expression was observed (p-value < 0.04): 21/67 genes (31.3%) were under-expressed and 46/67 genes (68.7%) are over-expressed in KO groups (Figure 1(D)). Similar to the EWAS analysis, our transcriptome-wide association study (TWAS) exhibited a high lambda value (lambda = 1.87), however, 500 null permutations identified the signal to be robust which indicates true signal (S4C-D Fig). Additionally, we demonstrate that reintroducing *TFAM* into *TFAM* KO cell lines leads to expected expression changes of selected differentially expressed genes identified via RNA sequencing (Figure 3). *TFAM* overexpression led to a significant increase in *TFAM* levels in both the KO and NC lines, however as one might expect, the increase was markedly larger in the KO lines compared to the NC lines (KO = 1.965 Ct difference, 3.90-fold increase, p-value = 9.29E-14; NC = 0.835 Ct difference, 1.78-fold increase, p-value = 4.09E-13) (Figure 3). To directly compare the magnitude of *TFAM* overexpression between KO lines and NC, we calculated the mean delta Ct difference between overexpression and non-overexpression samples for each line (NC and KO) and confirmed that the *TFAM* increase following overexpression was significantly greater in KO lines (KO = 1.975 mean Ct difference, NC = 0.839 mean Ct difference, 1.70-fold increase between NC and KO upon overexpression, p-value < 0.009) (Figure 3). We selected 8 genes from the RNA sequencing results to test for expression levels following *TFAM* reintroduction, our results identify corresponding gene expression changes in the expected direction of effect for at least 2 of the 3 KO lines for 6 of 8 DEGs (*CA2*, *CA8*, *RPL22l*, *DSEL*, *SLC16A2*, *SFRP2*) (Figure 3). The remaining genes (*ABCD1*, *FLRT2*) showed consistent trends in at least one KO line. Since our RNA sequencing results indicated no basal level of expression of *DSEL*, *FLRT2*, and *SFRP2* in the NC lines, only 5 of the 8 selected genes could be assessed (Figure 3). Of the 5 remaining tested genes in NC lines, *CA8* and *SLC16A2* displayed lower but expected differential expression in one, and two NC lines, respectively, upon *TFAM* re-introduction. Further, *RPL122L1* showed a consistent trend (*p*-value < 0.01) in the expected

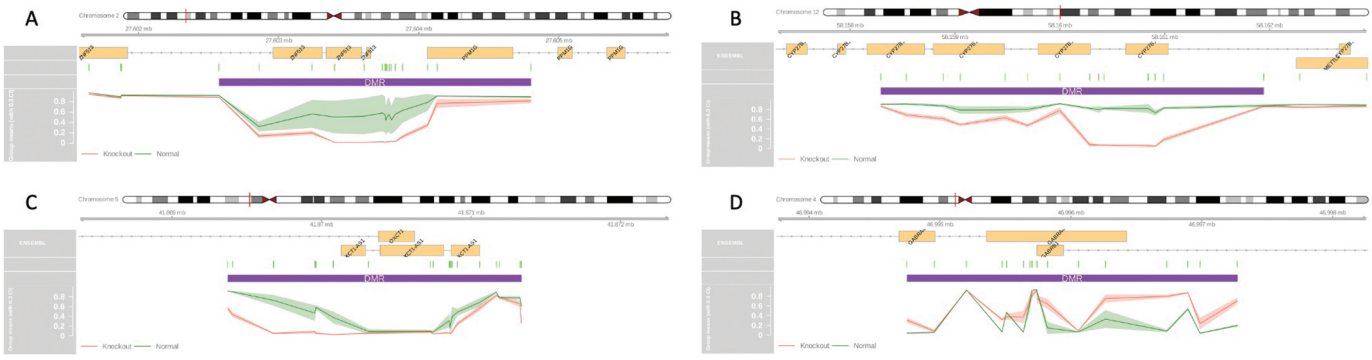

Figure 2. Representative Differentially Methylated Regions (DMRs). Pink represents *TFAM* KO groups, green represents negative control (NC) groups, colored clouds represent error. Rows represent biological replicates in a given group. (A) Protein Phosphatase, Mg2+/Mn2+ Dependent 1 G (*PPM1G*) related DMR, located on chromosome 2 (Fisher $p = 1.82e\text{-}78$). (B) cytochrome P450 family 27 subfamily B member 1 (*CYP27B1*) related DMR, located on chromosome 12 (Fisher $p = 5.92e\text{-}68$). (C) 3-oxoacid CoA-transferase 1 (*OXCT1*) related DMR, located on chromosome 5 (Fisher $p = 1.79e\text{-}73$). (D) Gamma-aminobutyric acid receptor subunit beta-1 (*GABRB1*) related DMR, located on chromosome 4 (Fisher $p = 3.82e\text{-}56$).

direction of effect for two NC lines, similar to the significant changes observed in the KO lines. The muted results in NC lines likely reflect the smaller *TFAM* fold change increase as compared to KO lines.

3.5. Integration of methylation and gene expression identifies CpG-gene interactions associated with TFAM KO

Since CpG sites near gene features can influence transcription [81], we investigated whether changes in DNA methylation at these sites are associated with nearby gene expression. To assess the relationship between differentially methylated sites and differentially expressed genes, we used the R package ELMER to integrate methylation and gene expression results for both direct and inverse associations between methylation at CpG sites and gene expression [60]. ELMER identified 524 possible Gene-CpG pairs from all tested CpGs and genes. Gene-CpG pairs were identified as those with differential methylation and gene expression between KO and NC witin 1 Mbp of one another (FDR < 0.05). Twenty-four gene-CpG pairs matched the filtering criteria established above, which included 14 unique genes and 23 unique CpG sites (S4 Table). Methylation and gene expression for the top 4 unique gene-CpG pairs, prioritized based on lowest p-values, were visualized (Figure 4). The top two identified gene-CpG pairs both belonged to genes encoding carbonic anhydrases. Both *CA2* and *CA8* genes were significantly downregulated in the gene expression analysis and further associated with hypomethylation at two significant CpG sites each (*CA2* with cg06015329; *CA8* with cg01756512 and cg13468096) (Figure 3(A,B)).

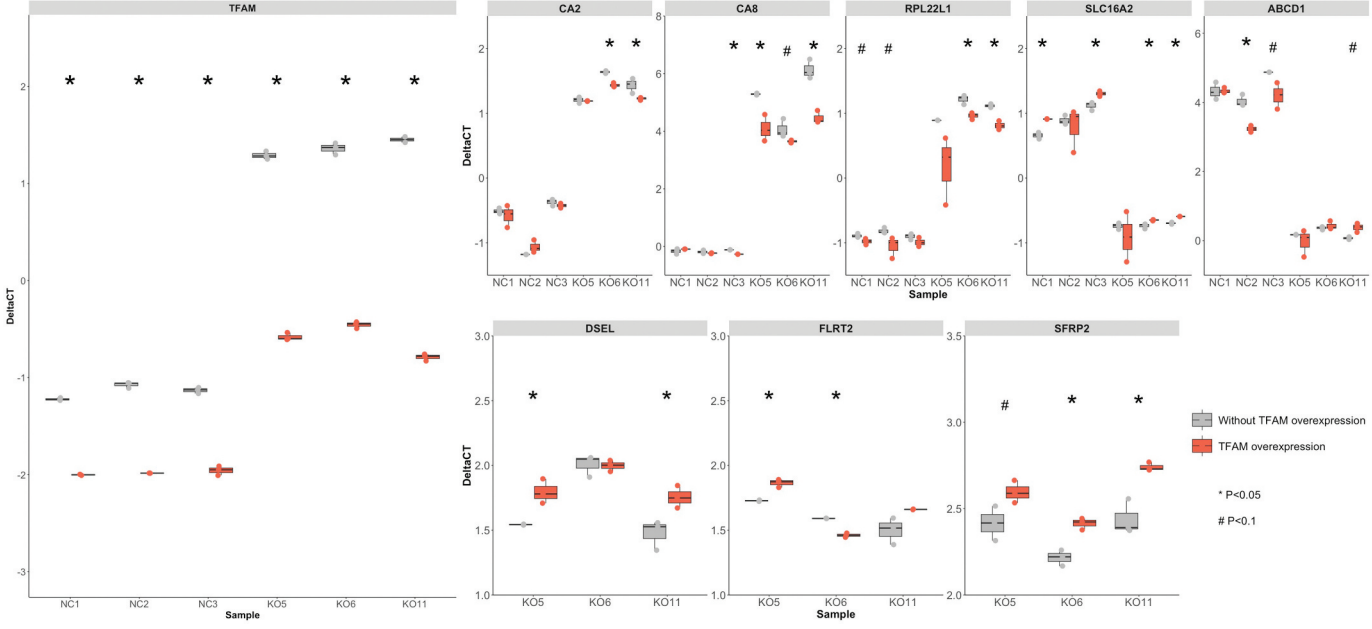

Figure 3. Gene expression following *TFAM* overexpression in *TFAM* KO and NC cell lines. Panels show relative gene expression levels for *TFAM* and eight differentially expressed genes (*CA2*, *CA8*, *RPL22L1*, *DSEL*, *SLC16A2*, *FLRT2*,*SFRP2*, *ABCD1*) in three independent *TFAM* KO cell lines after *TFAM* reintroduction and five of the genes in NC lines after *TFAM* reintroduction (due to there being no basal level expression for three of the genes). The *TFAM* gene was overexpressed using a plasmid via lipofection with Lipofectamine LTX. Delta Ct values were calculated as Target gene Ct – HPRT1 Ct, with replicates excluded for high variation between replicates. Results from one-tailed t-test between overexpression and non-overexpression condition indicated with * ($p < 0.05$) and # ($p < 0.1$).

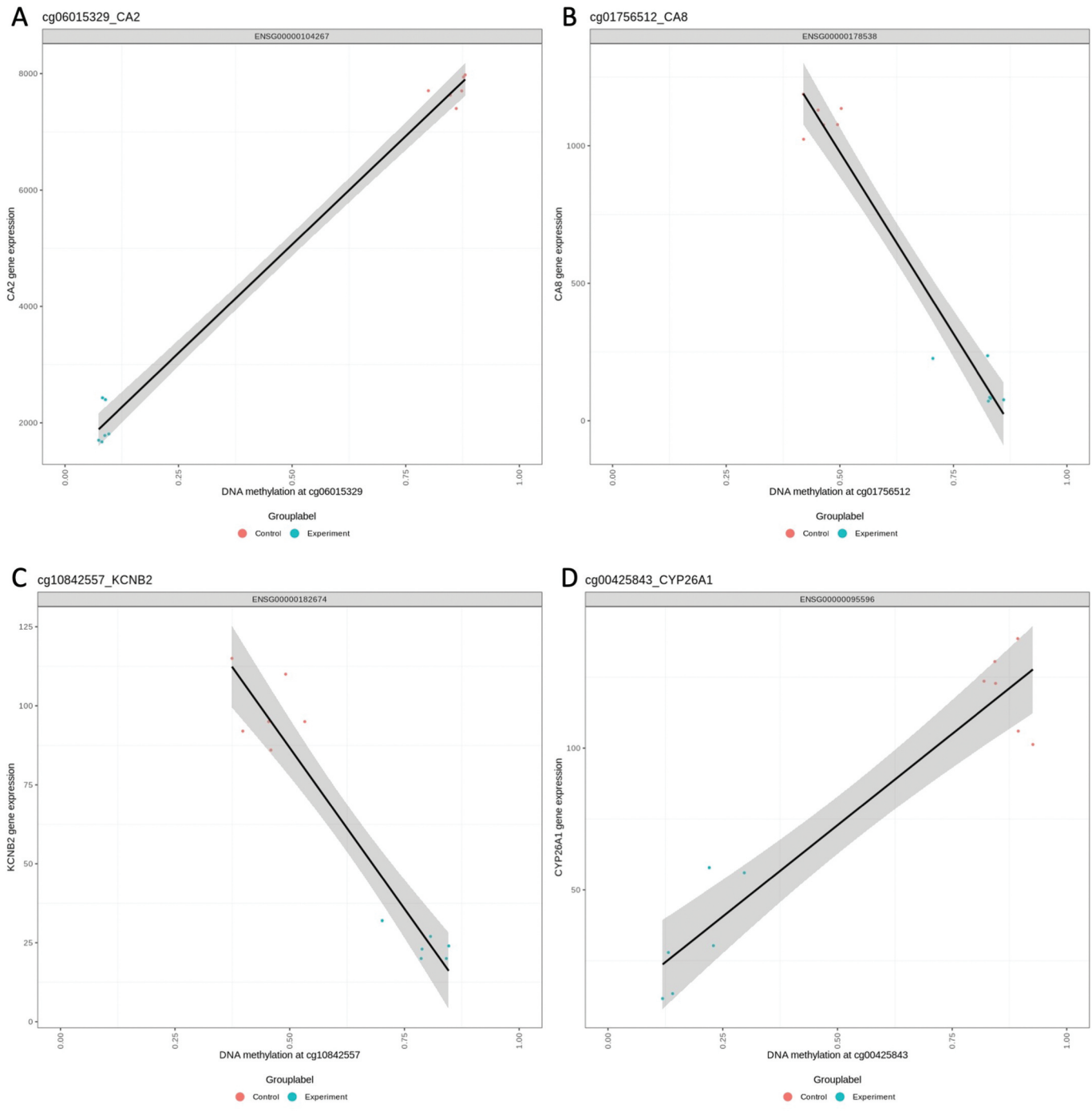

Figure 4. Top integrated methylation and gene expression results. (A) Association between Carbonic Anhydrase 2 (*CA2*) gene expression and methylation at cg06015329 (Pearson $R = 0.995$, p-value = 3.40E-10), identified as the top gene-CpG pair. (B) Association between Cabonic Anhydrase 8 (*CA8*) gene expression and methylation at cg01756512 (Pearson $R = 0.978$, p-value = 1.26E-9), identified as the second prioritized gene-CpG pair. (C) Association between Potassium Voltage-Gated Channel Subfamily B Member 2 (*KCNB2*) gene expression and methylation at cg10842557 (Pearson $R = 0.960$, p-value = 2.22E-6), identified as the third prioritized gene-CpG pair. (D) Association between Cytochrome P450 Family 26 Subfamily A Member 1 (*CYP26A1*) gene expression and methylation at cg00425843 (Pearson $R = 0.952$, p-value = 1.10E-5), identified as the fourth prioritized gene-CpG pair. Red corresponds to NC groups, blue corresponds to *TFAM* KO groups.

3.6. GABA and cell signaling-related genes are associated with TFAM knockout-induced differential methylation and gene expression

We hypothesized that *TFAM* KO-induced reduction in mtDNA-CN would alter nuclear epigenetic and gene expression profiles through disrupted mitochondrial metabolites and signaling pathways involved in mitochondrial-nuclear crosstalk. To characterize the functional consequences of these alterations and identify overrepresented biological themes that may mediate the effects of mtDNA-CN on disease-relevant processes, we performed GO analysis [63,64], KEGG enrichment [65–67], and Reactome analysis [74] across differentially methylated sites, DMRs, and differentially expressed genes.

The top GO terms for each of the three independent analyses include genes relating to GABA, plasma membrane components,

and signaling pathways (Figure 4(A–C)) (Table 1, S5-7 Tables). The GO Fisher's combined probability test, which was used to integrate significance values for differentially methylated sites/regions with differentially expressed genes, revealed enrichment for genes relating to plasma membrane, including integral component of cell periphery (Fisher *p*-value < 2.60e-10), and plasma membrane (Fisher *p*-value < 1.35e-08). GO term ligand-gated monoatomic anion channel activity (Fisher *p*-value < 2.30e-05) was also highlighted in our results. Additionally, several pathways related to GABA, including GABA-gated chloride ion channel activity (Fisher p-value < 3.77e-04), GABA receptor activity (Fisher *p*-value < 1.77e-03), $GABA_A$ receptor activity (Fisher *p*-value < 2.30e-03), and $GABA_A$ receptor complex (Fisher *p*-value < 2.30e-03) were overrepresented (Figure 5(D), Table 2). Differentially methylated region and gene expression results were enriched for GO terms relating to signaling pathways, including GABA receptor activity (Fisher *p*-value < 3.55e-03) and signaling receptor regulator activity (Fisher *p*-value < 5.43e-04) (Figure 5(E), Table 2). Taken together, these results implicate cell communication pathways as integral to these relationships. KEGG pathways identified from enrichment analyses of differentially methylated sites identify neuroactive ligand signaling to be overrepresented (S8 Table).

Major Reactome pathways identified from differentially expressed genes identify epigenetic regulation of gene expression including DNA methylation (FDR = 2.36e-5), histone modifications (FDR = 2.57e-6), and chromosome maintenance (FDR < 4.76e-5) (S5 Fig, S9 Table). No overrepresented Reactome pathways were identified from methylation results, therefore no combined analyses were performed.

3.7. TFAM knockout-associated methylation change identifies epigenetic enrichment in non-coding regions

Genomic region enrichment testing was performed to determine if CpG, gene, and chromatin state regions are overrepresented in our datasets. We discovered significant overrepresentation (FDR < 0.05) of intergenic regions, enhancers, zinc finger proteins (ZNF) genes and repeats, heterochromatin, bivalent TSS, flanking bivalent TSS/Enhancer, bivalent enhancer, repressed polyComb, weak repressed polyComb and quiescent/low group in the methylation dataset (S5 Fig, S10 Table). Conversely, the 5'UTR was under-enriched (FDR < 0.05) and overrepresentation of intergenic regions, different enhancer types, heterochromatin and repressed PolyComb regions was observed, implicating epigenetic marks in non-coding regions of the heterochromatic and enhancer region to be overrepresented. Non-coding regions including heterochromatin, open sea, and intergenic regions were significantly hypermethylated in *TFAM* KO (Chi-square FDR < 0.05), suggesting an increase in methylation may repress chromatin accessibility. Conversely, CpG shores, promoters, repressed PolyComb, bivalent/poised TSS, active TSS, and intronic regions were hypomethylated in *TFAM* KO samples (Chi-square FDR < 0.05). However, there were also other enriched terms of Bivalent Enhancer, Enhancers, Exon, 3'UTR, ZNF Genes & Repeat, Flanking Bivalent TSS/Enhancer, Weak Repressed PolyComb, and 5' UTR which did not show any significant directionality effect in DNA methylation.

To determine the intersection of our results with known protein-coding genes associated with mitochondrial proteins and pathways, we cross-referenced our gene set with the MitoCarta3.0 catalog. Top results from this MitoCarta3.0 analysis reveal mitochondrial dynamics and surveillance pathways to be implicated in our methylation results (FDR < 0.05). No overlapping pathways between methylation and gene expression results were identified in MitoCarta3.0 pathways and transcription factor genes. However, two (*ABCD1*, *ABCD2*) of 67 significant genes from the RNA analysis were found in the MitoCarta3.0 database of mitochondrial-related genes, and both genes were found to be underexpressed (FDR < 0.05).

4. Discussion

To determine the genes, regulatory sites, regions, and biological pathways associated with mtDNA-CN variation, we analyzed DNA methylation data from methylation microarrays and RNA sequencing data generated from cell lines with a heterozygous knockout

Table 1. Overrepresented gene ontology terms identified from Fisher's combined test of differentially methylated sites and differentially expressed genes.

	GO ID	Ontology	Term	N	DE	P.DE_Meth	P.DE_RNA	Fisher
1	GO:0071944	CC	Cell periphery	5938	498	1.35E-09	0.007327	2.60E-10
2	GO:0048731	BP	System development	4046	363	7.40E-07	0.000359	6.13E-09
3	GO:0005886	CC	Plasma membrane	5459	451	6.09E-08	0.009977	1.35E-08
4	GO:0007275	BP	Multicellular organism development	4733	403	2.51E-05	0.000801	3.76E-07
5	GO:0007399	BP	Nervous system development	2525	248	2.40E-06	0.022197	9.45E-07
6	GO:0072006	BP	Nephron development	158	22	0.006175	2.30E-05	2.38E-06
7	GO:0005882	CC	Intermediate filament	203	26	9.35E-06	0.027099	4.10E-06
8	GO:0099095	MF	Ligand-gated monoatomic anion channel activity	21	8	4.81E-05	0.033376	2.30E-05
9	GO:0042445	BP	Hormone metabolic process	239	23	0.026949	5.97E-05	2.31E-05
10	GO:0048856	BP	Anatomical structure development	5970	467	0.001669	0.001007	2.40E-05
11	GO:0010817	BP	Regulation of hormone levels	537	51	0.007672	0.000223	2.44E-05
12	GO:0032835	BP	Glomerulus development	71	11	0.02872	0.000113	4.44E-05
13	GO:0032501	BP	Multicellular organismal process	7773	567	0.002061	0.002022	5.58E-05
14	GO:0048513	BP	Animal organ development	3024	249	0.006516	0.001086	9.10E-05
15	GO:0062023	CC	Collagen-containing extracellular matrix	426	43	0.009529	0.001214	0.000143
16	GO:0072073	BP	Kidney epithelium development	152	21	0.008869	0.002382	0.000249
17	GO:0007267	BP	Cell-cell signaling	1712	155	0.002376	0.009662	0.000268
18	GO:0022851	MF	GABA-gated chloride ion channel activity	13	5	0.001735	0.019209	0.000377
19	GO:0043062	BP	Extracellular structure organization	329	37	0.008191	0.004188	0.000387
20	GO:0060485	BP	Mesenchyme development	330	37	0.00639	0.007264	0.00051

Abbreviations: BP: biological process; MF: molecular feature; CC: cellular component.

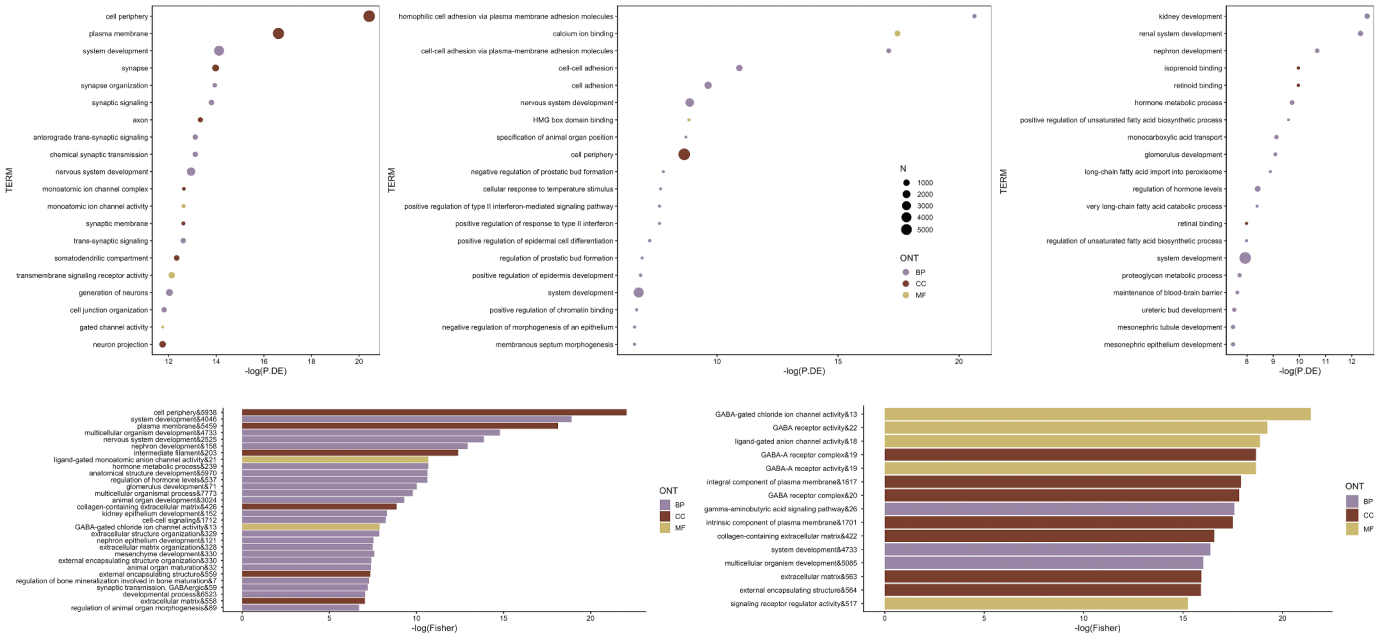

Figure 5. Top gene ontology (GO) terms identified. N: number of genes identified in each term; ONT: ontology; BP: biological process; CC: cellular components; MF: molecular function. (A) Terms identified from differentially methylated sites (FDR < 0.05). (B) Terms identified from differentially methylated regions (FDR < 0.05). (C) Terms identified from differentially expressed genes (FDR < 0.05). (D) Fisher's Combined results from methylation site and gene expression. (E) Fisher's Combined results from methylation region and gene expression.

of the *TFAM* gene. We report widespread differential methylation and differential gene expression in *TFAM* KO samples with reduced mtDNA-CN. The results specifically implicate regulation of carbonic anhydrases, cellular signaling, GABA receptors, neuroactive ligand signaling pathways, the *ABCD1* gene, and non-coding regulation as candidates for nuclear DNA methylation associated gene expression change.

4.1. GABA receptor and neuroactive ligand-related processes and pathways are associated with mtDNA-CN-induced nuclear genome modifications

The combined methylation and gene expression enrichment analyses identified numerous GABA-associated pathways, including GABA-gated chloride ion channel activity and GABA receptor activity. Additionally, GABAergic Synapse, ligand-gated monoatomic anion channel activity, plasma membrane and integral component of cell periphery pathways are overrepresented, and these pathways are all related to cell signaling. The methylation only analysis also identified neuroactive ligand signaling pathway to be enriched.

A previous study had found an association between the neuroactive ligand signaling pathway and blood-derived mtDNA-CN following a multi-ethnic EWAS meta-analysis across multiple independent human cohorts [25]. Association of the neuroactive ligand signaling pathway with phenotypic changes within kidney cells is exemplified by association with several

Table 2. Overrepresented gene ontology terms identified from Fisher's combined test of differentially methylated regions and differentially expressed genes.

	GO ID	Ontology	Term	N	DE	P.DE_Meth	P.DE_RNA	Fisher
1	GO:0001822	BP	Kidney development	319	6	0.023708	3.42E-06	1.40E-06
2	GO:0072001	BP	Renal system development	329	6	0.027288	4.40E-06	2.03E-06
3	GO:0072006	BP	Nephron development	158	5	0.005312	2.30E-05	2.06E-06
4	GO:0032835	BP	Glomerulus development	71	4	0.001791	0.000113	3.34E-06
5	GO:0048731	BP	System development	4046	42	0.001152	0.000359	6.50E-06
6	GO:0071944	CC	Cell periphery	5938	57	0.000176	0.007327	1.87E-05
7	GO:0007275	BP	Multicellular organism development	4733	46	0.002143	0.000801	2.45E-05
8	GO:0007399	BP	Nervous system development	2525	33	0.00014	0.022197	4.24E-05
9	GO:0062023	CC	Collagen-containing extracellular matrix	426	8	0.006357	0.001214	9.85E-05
10	GO:0048856	BP	Anatomical structure development	5970	50	0.019172	0.001007	0.000229
11	GO:0072111	BP	Cell proliferation involved in kidney development	22	2	0.011255	0.002646	0.00034
12	GO:0031012	CC	Extracellular matrix	558	9	0.010351	0.003913	0.00045
13	GO:0030312	CC	External encapsulating structure	559	9	0.010452	0.003913	0.000454
14	GO:0032501	BP	Multicellular organismal process	7773	60	0.021275	0.002022	0.000476
15	GO:0032502	BP	Developmental process	6523	55	0.009467	0.004859	0.000505
16	GO:0030545	MF	Signaling receptor regulator activity	549	8	0.011017	0.00452	0.000543
17	GO:0005886	CC	Plasma membrane	5459	48	0.005299	0.009977	0.000574
18	GO:0098594	CC	Mucin granule	2	1	0.010947	0.004837	0.000574
19	GO:0005201	MF	Extracellular matrix structural constituent	164	5	0.005187	0.011213	0.000625
20	GO:0072012	BP	Glomerulus vasculature development	30	2	0.018033	0.003736	0.000715

Abbreviations: BP: biological process; MF: molecular feature; CC: cellular component.

kidney-related diseases such as renal cell carcinoma [82], chronic renal failure [83], and diabetic nephropathy [84]. The neuroactive ligand signaling has also been associated with several age-related chronic diseases, including Alzheimer's disease [85], diabetic retinopathy [86], and various cancers [87–89]. The pathway is also linked to chemotherapy effectiveness in osteosarcoma [90]. Together, these studies provide further evidence that these changes are likely mediated through mtDNA-CN and that similar mechanisms may be involved.

GO results revealed enrichment for GABA and $GABA_A$ related gene groups in our dataset. The $GABA_A$ receptor is comprised of four subunit genes: *GABRB1*, *GABRB3*, *GABRE*, and *GABRG1* [91]. In our study, all four GABA receptor genes were significantly downregulated in the *TFAM* KO samples relative to the NC samples. In addition, integration analysis found the *GABRB1* gene to be associated with site-specific methylation at 13 CpGs. The $GABA_A$ receptor functions as a ligand-gated ion channel that allows for fast inhibitory synaptic transmission [91]. Reduced expression of $GABA_A$ receptor genes decreases the available receptors for GABA neurotransmitter binding, leading to overexcitation of the cell terminal neurons. Within kidney cells, the GABA system acts as a key regulator of the renal vasculature [92]. In pan-tissue investigations, the GABAergic signaling pathway has been shown to be associated with cancer progression [93], neurodevelopmental disorders [94–96], and has been identified as a target for diabetes treatment [97–99]. Additionally, the GABA neurotransmitter plays an important role in a variety of cellular processes such as suppressing inflammatory immune responses [100] and binding to islet alphas-cells to inhibit the secretion of glucagon [97]. Further, a mouse model study demonstrated mice lacking GABA-synthesizing genes die at birth despite no visible structural differences in their brains, suggesting further associated functions of GABA in neurodevelopment and animal physiology [91]. Taken together, the observed neural cell enrichment may stem from the established bidirectional mitochondrial-nuclear crosstalk, where mtDNA-CN reduction disrupts mitochondrial metabolites that influence nuclear DNA epigenetic and gene expression. Reduced mtDNA-CN in *TFAM* KO could lead to epigenetic regulation of neural signaling genes, such as *GABRB1*, *CA2*, and *CA8* as observed in our CpG-Gene integration analysis. These genes are critical for synaptic transmission and cellular homeostasis, potentially linking mtDNA-CN to neural dysfunction observed in age-related diseases like neurodegeneration [101]. However, as this was an exploratory analysis in the HEK293T cell line, further experimentation is required to fully elucidate the relationships of the identified associations to disease across a variety of cell types.

4.2. Mitochondrial-related genes are under-expressed in TFAM ko and associated with mtDNA-CN-induced DNA methylation and gene expression with implications for disease

The family of carbonic anhydrase (CA) enzymes are found in the mitochondria across tissue types where they elicit a variety of physiological functions [102]. CAII, encoded by the *CA2* gene, is involved in several pathological conditions including neurodegeneration, glaucoma, epilepsy, and altitude sickness, which has led to growing interest in the clinical use of carbonic anhydrase inhibitors [103–105]. Patients with osteopetrosis and renal tubular acidosis were discovered to carry mutations resulting in the downregulation of CAII [106]. These manifestations are also observed in inherited autosomal recessive CAII deficiency syndrome [107]. CAVIII, encoded by the *CA8* gene, is another carbonic anhydrase isoform that is downregulated in renal cell carcinoma [108] and congenital ataxia [109]. Our results found both *CA2* and *CA8* to be downregulated following *TFAM* KO and associated with hypomethylation at 2 unique CpG sites each (4 CpG sites total) (S4 Table).

The *ABCD1* gene functions as an ATP-binding cassette transporter which helps move very long chain fatty acid-CoA from the cytosol to the peroxisome [110,111]. Additionally, the *ABCD1* gene also regulates mitochondrial-related functions such as oxidative phosphorylation and fatty acid synthesis [110,111]. The X-linked adrenoleukodystrophy genetic peroxisome disease has been linked to mutations in the *ABCD1* gene, which affects the nervous system and kidney [112,113]. Our gene expression results identify the *ABCD1* gene and it is also included in the MitoCarta3.0 database. The *ABCD1* gene is also associated with 9 significant CpG sites from our dataset (S4 Table). Furthermore, *ABCD1*, and its paralog *ABCD2*, are both underexpressed in our analysis and only the metabolism pathway overlapped between the MitoCarta3.0 database and the overrepresented pathways from the gene expression analysis. mtDNA-CN reduction following *TFAM* KO may lead to *ABCD1* hypermethylation, resulting in decreased expression and consequently altered energy metabolism. Further investigations on a potential association between mtDNA-CN alterations and *ABCD1*-related diseases such as X-linked adrenoleukodystrophy is warranted [114].

4.3. mtDNA-CN reduction is related to the enrichment of non-coding chromatin regions

Enrichment in chromatin state regions such as enhancers and repressed Polycomb was identified in our analyses. These findings may suggest the existence of interaction between mtDNA-CN and the machinery regulating chromatin states as another avenue of mitochondrial-nuclear crosstalk, with potential implications on disease etiology. Further investigations of the associations between mtDNA-CN and chromatin states by leveraging ATAC-seq or ChIP-seq is warranted. CpG islands and CpG shelves display underenrichment, indicating that differential methylation is less frequent in these gene-regulatory regions. Additionally, enrichment in Open Sea could influence long-range chromatin interactions or nuclear architecture, indirectly affecting nuclear genes involved in mitochondrial biogenesis or function, such as *TFAM* or *POLG* [26]. The enrichment for intergenic regions in our dataset follows another mtDNA-CN-modifying investigation that found DMRs overrepresented in intragenic regions, with the majority found in introns [115]. These findings further suggest gene expression control is being regulated through non-coding regions. Taken together, our results may indicate that epigenetic changes in non-coding regions of the genome, specifically those associated with heterochromatin and

enhancer elements, may play a role in modulating mtDNA-nuclear crosstalk. Hypermethylation of heterochromatin in *TFAM* KO is consistent with prior evidence suggesting that increased methylation in such regions can impact chromatin accessibility, while hypomethylation of TSS and promoter regions may facilitate compensatory transcriptional regulation, potentially mediating changes in nuclear-mitochondrial communication. Additionally, under-enrichment of the 5'UTR may further suggest that regulatory mechanisms outside coding regions may be central to our results. Consistent with these findings, our enrichment analysis revealed that differentially methylated CpG sites were significantly overrepresented in intergenic and non-coding chromatin regions – including enhancers, heterochromatin, and Polycomb domains – while promoter- and CpG shore-associated regions tended to be underenriched. A similar observation was also seen in previous studies where mitochondrial stress remodeled chromatin structure and enhancer accessibility through metabolite-driven methylation changes [113,116,117], supporting the notion that *TFAM* KO – induced mtDNA-CN reduction selectively alters methylation within non-coding regulatory elements to influence nuclear transcriptional output.

4.4. mtDNA-CN remodels the nuclear epigenome and transcriptome

Our results, alongside emerging evidence on the association between mtDNA variability, the nuclear epigenome, and nuclear gene expression, reinforce the complex interplay between the mitochondria and the nuclear genome [48,118,119]. *TFAM* knockout reduces mtDNA-CN and alters nDNA methylation and gene expression. Environmental stimuli could influence these changes via mitochondrial-nuclear genome cross-talk [120], mediated by metabolites of the methionine cycle, like SAM [42], that donates the methyl group during DNA methylation [116,121]. The methionine cycle also consists of S-adenosylhomocysteine (SAH), homocysteine, and methionine, which mediates mito-nuclear crosstalk [117,121]. Metabolites belonging to the TCA cycle, OXPHOS, and folate/one-carbon cycle, such as methylthioadenosine (MTA), alpha-ketoglutarate, serine, choline, NADH, and betaine are also associated with DNA methylation [31,44,117,122–124]. In addition, *TFAM* KO induced mtDNA-CN depletion via nucleoid instability enhances mitochondrial reactive oxygen species (mtROS) signaling. *TFAM* is critical for nucleoid formation [125–127], and its loss disrupts nucleoid integrity [128], while elevated mtROS in tumor cells [129] further contributes to these changes providing another possible mechanism in which the *TFAM* KO model may remodel the epigenome and transcriptome. *TFAM* KO induced mtDNA-CN reduction may therefore lead to increased mitochondrial reactive oxygen species, disrupted metabolite pools of S-adenosylmethionine, and nucleoid instability [116,130,131]. Differential methylation of CpGs and differential gene expression in *GABRB1, CA2, CA8*, and *ABCD1* may be one of the leading causes of observed dysregulation. Changes in regulation of pathways associated with these genes such as GABA receptor activity and neuroactive ligand signaling may be particularly sensitive to mitochondrial stress signals. These connections are further supported by prior studies showing that mtDNA depletion influences nuclear DNA methylation and gene expression via metabolite availability and ROS signaling.

Reintroduction of *TFAM* via overexpression led to significant changes in gene expression in the expected direction for the majority of selected differentially expressed genes identified from RNA sequencing, including *CA2*, *CA8*, *RPL22L1*, *DSEL*, *SLC16A2*, and *SFRP2*. In contrast, *TFAM* overexpression in untreated NC lines produced more modest *TFAM* expression changes, in the same direction of effect as seen in *TFAM* KO, however, these changes were not always large enough to be statistically significant. Expression changes in the *TFAM* KO cells have therefore likely arisen due to *TFAM* depletion and its downstream effects on mtDNA-CN. However, as expected some variability is seen, likely reflecting the heterogenous nature of the cellular dynamics underpinning these relationships. A limitation of the TFAM overexpression experiment is the 48-hour *TFAM* re-introduction period, which resulted in incomplete restoration of basal levels for several downstream genes (Figure 3). Studies with longer periods of re-introduction will be required to establish whether full restoration is achievable for these targets. Here, we identify biological pathways in relation to these associations and highlight key targets for further research. These findings provide insight on anticipated effects to the nuclear epigenome and nuclear genome expression as a result of mtDNA modifications. Some limitations of these results include cell line considerations, the kidney-derived HEK293T cell line was edited to create the *TFAM* KO and NC cell lines due to their availability of optimized protocols for CRISPR-Cas9 as well as their propensity for transfection. However, immortalized cancer cell lines, like HEK293T, are inherently heterogeneous and prone to karyotypic abnormalities with a high level of clonality expected across individual clones [132]. The established cell lines may also have a bias to specific pathways since they are transformed cells, potentially limiting their generalizability to other cell types. Additionally, despite consistent mtDNA-CN stability across passages and concordant methylation signals from two passages, the use of different passages for DNA methylation (P32 & P37) and RNA sequencing analyses (P45) represents a limitation of this study. Therefore, the findings of this study are not expected to be generalizable to all cell types. However, HEK293T cells are still a popular first choice model to investigate the effects of disease in culture, including studies of metabolic diseases [133], type 2 diabetes [134], osteoarthritis [135], and others. However, we note that the use of a primary cell line may be more relevant to aid in the direct interpretation of the results and therefore should be considered as an essential next step to extend these findings, particularly given that we were not able to identify any overlaps between CpGs in this study and previous EWAS studies on mtDNA-CN in blood. Further, *TFAM* KO cells have resulted in a more substantial reduction in mtDNA-CN compared to what is generally observed in human patients and should therefore be interpreted with caution. Despite high on-target efficiency of our *TFAM* gene knockout and consistent results across three independent knockouts, as well as no identified off-target edits identified across eight predicted loci, there still

remains the potential for off-target effects stemming from the inherent nature of the CRISPR-Cas9 system, which represents a potential limitation of the use of this technology. Additionally, the *TFAM* gene may also independently impact other pathways, such as inducing mtDNA release to the cytosol and activating an inflammatory pathway in addition to regulating mtDNA-CN which in turn could impact nDNA methylation and gene expression through other biological mechanisms, thus additional models will be needed to further delineate these relationships.

5. Conclusion

In conclusion, we report the impact of reduction of *TFAM* on site-specific differential DNA methylation, differentially methylated regions, and differential gene expression. Overrepresentation of $GABA_A$ receptor genes, the neuroactive ligand signaling pathway, the *ABCD1/2* genes, regulation of carbonic anhydrases, and cell signaling processes were identified. Furthermore, enrichment of functional genomic regions demonstrated that chromatin states such as enhancers and heterochromatin are overrepresented in the methylation results, implying that mtDNA-CN may also be impacting gene expression via chromatin states. The results indicate that mitochondrial DNA variation influences the nuclear DNA epigenome and transcriptome and has the potential to contribute to processes related to development, aging, and complex disease risk.

Acknowledgments

We acknowledge the London Regional Genomics Centre for their assistance with DNA sequencing for off-target analysis. We also acknowledge Anna Ciurzynska and Shamaila Rahman, Molecular Diagnostics Division, London Health Sciences Centre, London, Ontario, for technical assistance with karyotyping. We further acknowledge Dr. Kathleen A. Hill for equipment support.

Author contributions

Christina A. Castellani, Dan E. Arking, Gregory Newby, and Charles Newcomb, conceived and designed the experiments. Phyo W. Win, Julia Nguyen, Elly H. Shin, Tyler S. Nagano, Brent Selimi, Katie Hong, Anahita M. Meybodi, David Carter, Bradley P. Yates, Emma V. Burke, Gregory A. Newby, Charles Newcomb, Dan E. Arking, and Christina A. Castellani acquired, analyzed, and interpreted the data. Julia Nguyen, Phyo W. Win, and Tyler S. Nagano were responsible for the drafting of the manuscript. Charles Newcomb, Elly H. Shin, Christina A. Castellani, and Dan E. Arking critically revised the manuscript for important intellectual content. Phyo E. Win, Julia Nguyen, Tyler S. Nagano, and Christina A. Castellani performed statistical analysis. Christina A. Castellani and Dan E. Arking obtained funding, provided administrative, technical, and material support. All authors read and approved the final manuscript.

Disclosure statement

The authors have no relevant affiliations or financial involvement with any organization or entity with a financial interest in or financial conflict with the subject matter or materials discussed in the manuscript. This includes employment, consultancies, honoraria, stock ownership or options, expert testimony, grants or patents received or pending, or royalties.

No writing assistance was utilized in the production of this manuscript.

Reviewer disclosures

Peer reviewers on this manuscript have no relevant financial or other relationships to disclose.

Ethical declaration

This study follows the principles of the Declaration of Helsinki. All experiments conducted were approved by Western University's Biosafety committee.

Funding

This manuscript was funded by the Department of Pathology and Laboratory Medicine at Western University, Western University Internal Support, The Children's Health Research Institute (CHRI), Ontario Graduate Scholarship (OGS), and The National Institutes of Health (NIH) grants R01HL14469, R01HL144569, and R00HL163805.

Data availability statement

The cell line datasets analyzed for the current study are available in the NCBI Gene Expression Omnibus repository (GEO; http://www.ncbi.nlm.nih.gov/geo/) under accession numbers GSE133994 and GSE134048.

References

Papers of special note have been highlighted as either of interest (•) or of considerable interest (••) to readers.

1. Butow RA, Avadhani NG. Mitochondrial Signaling. Mol Cell. 2004;14(1):1–15. doi: 10.1016/S1097-2765(04)00179-0
2. Knez J, Winckelmans E, Plusquin M, et al. Correlates of peripheral blood mitochondrial DNA content in a General population. Am J Epidemiol. 2015:kwv175. doi: 10.1093/aje/kwv175
3. Jeng J-Y, Yeh T-S, Lee J-W, et al. Maintenance of mitochondrial DNA copy number and expression are essential for preservation of mitochondrial function and cell growth. J Cell Biochem. 2008;103(2):347–357. doi: 10.1002/jcb.21625
4. Dai D-F, Rabinovitch PS, Ungvari Z. Mitochondria and cardiovascular aging. Sinclair d, north B, editors. Circ Res. 2012;110(8):1109–1124. doi: 10.1161/CIRCRESAHA.111.246140
5. Ashar FN, Zhang Y, Longchamps RJ, et al. Association of mitochondrial DNA copy number with cardiovascular disease. JAMA Cardiol. 2017;2(11):1247. doi: 10.1001/jamacardio.2017.3683
6. Chen S, Xie X, Wang Y, et al. Association between leukocyte mitochondrial DNA content and risk of coronary heart disease: a case-control study. Atherosclerosis. 2014;237(1):220–226. doi: 10.1016/j.atherosclerosis.2014.08.051
7. Liu X, Longchamps RJ, Wiggins KL, et al. Association of mitochondrial DNA copy number with cardiometabolic diseases. Cell Genomics. 2021;1(1):100006. doi: 10.1016/j.xgen.2021.100006
8. Tin A, Grams ME, Ashar FN, et al. Association between mitochondrial DNA copy number in peripheral blood and incident CKD in the atherosclerosis risk in communities study. J Am Soc Nephrol. 2016;27(8):2467–2473. doi: 10.1681/ASN.2015060661
9. Jin L, Yu B, Armando I, et al. Mitochondrial DNA-Mediated inflammation in acute kidney injury and chronic kidney disease. Immenschuh S, editor. Oxid Med Cell Longev. 2021;2021(1):1–12. doi: 10.1155/2021/9985603
10. Cocco MP, White E, Xiao S, et al. Asthma and its relationship to mitochondrial copy number: results from the asthma translational Genomics collaborative (ATGC) of the trans-omics for precision Medicine (TOPMed) program. Mersha TB, editor. PLOS ONE. 2020;15(11):e0242364. doi: 10.1371/journal.pone.0242364
11. Liu S-F, Kuo H-C, Tseng C-W, et al. Leukocyte mitochondrial DNA copy number is associated with chronic obstructive pulmonary disease. Su Y, editor. PLOS ONE. 2015;10(9):e0138716. doi: 10.1371/journal.pone.0138716

12. Arruda AP, Pers BM, Parlakgül G, et al. Chronic enrichment of hepatic endoplasmic reticulum–mitochondria contact leads to mitochondrial dysfunction in obesity. Nat Med. 2014;20 (12):1427–1435. doi: 10.1038/nm.3735
13. Reznik E, Miller ML, Şenbabaoğlu Y, et al. Mitochondrial DNA copy number variation across human cancers. Elife. 2016;5:e10769. doi: 10.7554/eLife.10769
14. Sun X, Zhan L, Chen Y, et al. Increased mtDNA copy number promotes cancer progression by enhancing mitochondrial oxidative phosphorylation in microsatellite-stable colorectal cancer. Signal Transduct Target Ther. 2018;3(1):8. doi: 10.1038/s41392-018-0011-z
15. Dang CV. Links between metabolism and cancer. Genes Dev. 2012;26(9):877–890. doi: 10.1101/gad.189365.112
16. Abd Radzak SM, Mohd Khair SZ, Ahmad F, et al. Insights regarding mitochondrial DNA copy number alterations in human cancer (review). Int J Mol Med. 2022;50(2):104. doi: 10.3892/ijmm.2022.5160
17. Yang SY, Castellani CA, Longchamps RJ, et al. Blood-derived mitochondrial DNA copy number is associated with gene expression across multiple tissues and is predictive for incident neurodegenerative disease. Genome Res. 2021;31(3):349–358. doi: 10.1101/gr.269381.120

•• **This study highlights the association between mtDNA-CN variation and gene expression and how it affects risk of incident neurodegenerative disease.**

18. Fazzini F, Lamina C, Raftopoulou A, et al. Association of mitochondrial DNA copy number with metabolic syndrome and type 2 diabetes in 14 176 individuals. J Intern Med. 2021;290(1):190–202. doi: 10.1111/joim.13242
19. Ashar FN, Moes A, Moore AZ, et al. Association of mitochondrial DNA levels with frailty and all-cause mortality. J Mol Med. 2015;93 (2):177–186. doi: 10.1007/s00109-014-1233-3

• **This study highlights the association of mtDNA-CN and all-cause mortality.**

20. Portela A, Esteller M. Epigenetic modifications and human disease. Nat Biotechnol. 2010;28(10):1057–1068. doi: 10.1038/nbt.1685
21. Li E, Beard C, Jaenisch R. Role for DNA methylation in genomic imprinting. Nature. 1993;366(6453):362–365. doi: 10.1038/366362a0
22. Cagin U, Enriquez JA. The complex crosstalk between mitochondria and the nucleus: what goes in between? Int J Biochem Cell Biol. 2015;63:10–15. doi: 10.1016/j.biocel.2015.01.026
23. Delsite R, Kachhap S, Anbazhagan R, et al. Nuclear genes involved in mitochondria-to-nucleus communication in breast cancer cells. Mol Cancer. 2002;1(1):6. doi: 10.1186/1476-4598-1-6
24. Smiraglia D, Kulawiec M, Bistulfi GL, et al. A novel role for mitochondria in regulating epigenetic modifications in the nucleus. Cancer Biol Ther. 2008;7(8):1182–1190. doi: 10.4161/cbt.7.8.6215
25. Castellani CA, Longchamps RJ, Sumpter JA, et al. Mitochondrial DNA copy number can influence mortality and cardiovascular disease via methylation of nuclear DNA CpGs. Genome Med. 2020;12 (1):84. doi: 10.1186/s13073-020-00778-7

•• **This paper shows methylation changes at specific nDNA CpG sites upon mtDNA-CN variation in three different human cohorts, followed by the experimental modification of mtDNA-CN through heterozygous knockout of TFAM using CRISPR-dCas9 to assess downstream global methylation and gene expression changes.**

26. Wang P, Castellani CA, Yao J, et al. Epigenome-wide association study of mitochondrial genome copy number. Hum Mol Genet. 2021;31(2):309–319. doi: 10.1093/hmg/ddab240

•• **This meta-analysis of human cohort data identifies that mtDNA-CN variation is associated with site-specific methylation level changes at several CpG sites.**

27. Guantes R, Rastrojo A, Neves R, et al. Global variability in gene expression and alternative splicing is modulated by mitochondrial content. Genome Res. 2015;25(5):633–644. doi: 10.1101/gr.178426.114
28. Spyrou J, Gardner DK, Harvey AJ. Metabolomic and transcriptional analyses reveal atmospheric oxygen during human induced pluripotent stem cell generation impairs metabolic reprogramming. STEM Cells. 2019;37(8):1042–1056. doi: 10.1002/stem.3029
29. Bellizzi D, D'Aquila P, Giordano M, et al. Global DNA methylation levels are modulated by mitochondrial DNA variants. Epigenomics. 2012;4(1):17–27. doi: 10.2217/epi.11.109

• **This study highlights the impact of mtDNA variation on global DNA methylation through cybrid models with different haplogroups.**

30. Lee WT, Sun X, Tsai T-S, et al. Mitochondrial DNA haplotypes induce differential patterns of DNA methylation that result in differential chromosomal gene expression patterns. Cell Death Discov. 2017;3 (1):17062. doi: 10.1038/cddiscovery.2017.62
31. Kopinski PK, Janssen KA, Schaefer PM, et al. Regulation of nuclear epigenome by mitochondrial DNA heteroplasmy. Proc Natl Acad Sci. 2019;116(32):16028–16035. doi: 10.1073/pnas.1906896116
32. Vivian CJ, Brinker AE, Graw S, et al. Mitochondrial genomic backgrounds affect nuclear DNA methylation and gene expression. Cancer Res. 2017;77(22):6202–6214. doi: 10.1158/0008-5472.CAN-17-1473

•• **Mitochondrial Nuclear Exchange mouse models show that alterations of mtDNA in nDNA-identical strains show differential genome-wide nDNA methylation and gene expression in brain tissues.**

33. Campbell CT, Kolesar JE, Kaufman BA. Mitochondrial transcription factor a regulates mitochondrial transcription initiation, DNA packaging, and genome copy number. Biochim Biophys Acta BBA - Gene Regul Mech. 2012;1819(9–10):921–929. doi: 10.1016/j.bbagrm.2012.03.002
34. Kang I, Chu CT, Kaufman BA. The mitochondrial transcription factor TFAM in neurodegeneration: emerging evidence and mechanisms. FEBS Lett. 2018;592(5):793–811. doi: 10.1002/1873-3468.12989

• **This review highlights the role of TFAM in mtDNA genome maintenance and the potential TFAM-associated effect of mtDNA variation on neurodegenerative diseases such as Alzheimer's Disease, Parkinson's Disease, and Huntington Disease.**

35. Larsson N-G, Wang J, Wilhelmsson H, et al. Mitochondrial transcription factor a is necessary for mtDNA maintance and embryogenesis in mice. Nat Genet. 1998;18(3):231–236. doi: 10.1038/ng0398-231
36. Li H, Wang J, Wilhelmsson H, et al. Genetic modification of survival in tissue-specific knockout mice with mitochondrial cardiomyopathy. Proc Natl Acad Sci. 2000;97(7):3467–3472. doi: 10.1073/pnas.97.7.3467
37. Otten ABC, Kamps R, Lindsey P, et al. Tfam knockdown results in reduction of mtDNA copy number, OXPHOS deficiency and abnormalities in zebrafish embryos. Front Cell Dev Biol. 2020;8:381. doi: 10.3389/fcell.2020.00381
38. Vernochet C, Mourier A, Bezy O, et al. Adipose-specific deletion of TFAM increases mitochondrial oxidation and protects mice against obesity and insulin resistance. Cell Metab. 2012;16(6):765–776. doi: 10.1016/j.cmet.2012.10.016
39. Lu T, Zhang Z, Bi Z, et al. TFAM deficiency in dendritic cells leads to mitochondrial dysfunction and enhanced antitumor immunity through cGAS-STING pathway. J Immunother Cancer. 2023;11(3): e005430. doi: 10.1136/jitc-2022-005430
40. Qi Y, Ye Y, Wang R, et al. Mitochondrial dysfunction by TFAM depletion disrupts self-renewal and lineage differentiation of human PSCs by affecting cell proliferation and YAP response. Redox Biol. 2022;50:102248. doi: 10.1016/j.redox.2022.102248
41. Stiles AR, Simon MT, Stover A, et al. Mutations in TFAM, encoding mitochondrial transcription factor a, cause neonatal liver failure associated with mtDNA depletion. Mol Genet Metab. 2016;119(1):91–99.
42. Morin AL, Win PW, Lin AZ, et al. Mitochondrial genomic integrity and the nuclear epigenome in health and disease. Front Endocrinol. 2022;13. doi: 10.3389/fendo.2022.1059085
43. Caracausi M, Ramacieri G, Catapano F, et al. The functional roles of S-adenosyl-methionine and S-adenosyl-homocysteine and their

involvement in trisomy 21. Biofactors. 2024;50(4):709–724. doi: 10.1002/biof.2044
44. Lozoya OA, Wang T, Grenet D, et al. Mitochondrial acetyl-CoA reversibly regulates locus-specific histone acetylation and gene expression. Life Sci Alliance. 2019;2(1):e201800228. doi: 10.26508/lsa.201800228
45. Fu Z, Ye J, Dean JW, et al. Requirement of mitochondrial transcription factor a in tissue-resident regulatory T cell maintenance and function. Cell Rep. 2019;28(1):159–171.e4. doi: 10.1016/j.celrep.2019.06.024
46. Hansson A, Hance N, Dufour E, et al. A switch in metabolism precedes increased mitochondrial biogenesis in respiratory chain-deficient mouse hearts. Proc Natl Acad Sci. 2004;101(9):3136–3141. doi: 10.1073/pnas.0308710100
47. Smiraglia DJ, Kulawiec M, Bistulfi GL, et al. A novel role for mitochondria in regulating epigenetic modification in the nucleus. Cancer Biol Ther. 2008;7(8):1182–1190.
48. Sharma N, Pasala MS, Prakash A. Mitochondrial DNA: epigenetics and environment. Environ Mol Mutagen. 2019;60(8):668–682. doi: 10.1002/em.22319
49. Santos JH. Mitochondria signaling to the epigenome: a novel role for an old organelle. Free Radic Biol Med. 2021;170:59–69. doi: 10.1016/j.freeradbiomed.2020.11.016
50. Huang TP, Newby GA, Liu DR. Precision genome editing using cytosine and adenine base editors in mammalian cells. Nat Protoc. 2021;16(2):1089–1128. doi: 10.1038/s41596-020-00450-9
51. Clement K, Rees H, Canver MC, et al. CRISPResso2 provides accurate and rapid genome editing sequence analysis. Nat Biotechnol. 2019;37(3):224–226. doi: 10.1038/s41587-019-0032-3
52. Aryee MJ, Jaffe AE, Corrada-Bravo H, et al. Minfi: a flexible and comprehensive Bioconductor package for the analysis of infinium DNA methylation microarrays. Bioinformatics. 2014;30(10):1363–1369. doi: 10.1093/bioinformatics/btu049
53. Fortin J-P, Triche TJ, Hansen KD. Preprocessing, normalization and integration of the Illumina HumanMethylationEPIC array with minfi. Hancock j, editor. Bioinformatics. 2017;33(4):558–560. doi: 10.1093/bioinformatics/btw691
54. Pidsley R, Zotenko E, Peters TJ, et al. Critical evaluation of the Illumina MethylationEPIC BeadChip microarray for whole-genome DNA methylation profiling. Genome Biol. 2016;17(1):208. doi: 10.1186/s13059-016-1066-1
55. Peters TJ, Buckley MJ, Statham AL, et al. De Novo identification of differentially methylated regions in the human genome. Epigenet Chromatin. 2015;8(1):6. doi: 10.1186/1756-8935-8-6
56. Bray NL, Pimentel H, Melsted P, et al. Erratum: near-optimal probabilistic RNA-seq quantification. Nat Biotechnol. 2016;34(8):888–888. doi: 10.1038/nbt0816-888d
57. Robinson MD, McCarthy DJ, Smyth GK. edgeR: a Bioconductor package for differential expression analysis of digital gene expression data. Bioinformatics. 2010;26(1):139–140. doi: 10.1093/bioinformatics/btp616
58. Robinson MD, Oshlack A. A scaling normalization method for differential expression analysis of RNA-seq data. Genome Biol. 2010;11(3):R25. doi: 10.1186/gb-2010-11-3-r25
59. Chen Y, Lun ATL, Smyth GK. Differential expression analysis of complex RNA-seq experiments using edgeR. In: Datta S, Nettleton D, editors. Stat Anal Gener Seq Data [Internet]. Cham: Springer International Publishing; 2014 [cited 2023 May 9]. p. 51–74. Available from: https://doi.org/10.1007/978-3-319-07212-8_3
60. Silva TC, Coetzee SG, Gull N, et al. ELMER v.2: an R/Bioconductor package to reconstruct gene regulatory networks from DNA methylation and transcriptome profiles. Stegle O, editor. Bioinformatics. 2019;35(11):1974–1977. doi: 10.1093/bioinformatics/bty902
61. Yates A, Akanni W, Amode MR, et al. Ensembl 2016. Nucleic Acids Res. 2016;44(D1):D710–D716. doi: 10.1093/nar/gkv1157
62. Yao C, Joehanes R, Wilson R, et al. Epigenome-wide association study of whole blood gene expression in framingham heart study participants provides molecular insight into the potential role of CHRNA5 in cigarette smoking-related lung diseases. Clin Epigenet. 2021;13(1):60. doi: 10.1186/s13148-021-01041-5
63. Ashburner M, Ball CA, Blake JA, et al. Gene ontology: tool for the unification of biology. Nat Genet. 2000;25(1):25–29. doi: 10.1038/75556
64. Carbon S, Douglass E, Good BM, et al. The gene ontology resource: enriching a GOld mine. Nucleic Acids Res. 2021;49(D1):D325–D334. doi: 10.1093/nar/gkaa1113
65. Kanehisa M. KEGG: kyoto encyclopedia of genes and genomes. Nucleic Acids Res. 2000;28(1):27–30. doi: 10.1093/nar/28.1.27
66. Kanehisa M. Toward understanding the origin and evolution of cellular organisms. Protein Sci. 2019;28(11):1947–1951. doi: 10.1002/pro.3715
67. Kanehisa M, Furumichi M, Sato Y, et al. KEGG: integrating viruses and cellular organisms. Nucleic Acids Res. 2021;49(D1):D545–D551. doi: 10.1093/nar/gkaa970
68. Liberzon A, Birger C, Thorvaldsdóttir H, et al. The molecular signatures database hallmark gene set collection. Cell Syst. 2015;1(6):417–425. doi: 10.1016/j.cels.2015.12.004
69. Subramanian A, Tamayo P, Mootha VK, et al. Gene set enrichment analysis: a knowledge-based approach for interpreting genome-wide expression profiles. Proc Natl Acad Sci. 2005;102(43):15545–15550. doi: 10.1073/pnas.0506580102
70. Rath S, Sharma R, Gupta R, et al. MitoCarta3.0: an updated mitochondrial proteome now with sub-organelle localization and pathway annotations. Nucleic Acids Res. 2021;49(D1):D1541–D1547. doi: 10.1093/nar/gkaa1011
71. Phipson B, Maksimovic J, Oshlack A. missMethyl: an R package for analyzing data from Illumina's HumanMethylation450 platform. Bioinformatics. 2016;32(2):286–288. doi: 10.1093/bioinformatics/btv560
72. Young MD, Wakefield MJ, Smyth GK, et al. Gene ontology analysis for RNA-seq: accounting for selection bias. Genome Biol. 2010;11(2):R14. doi: 10.1186/gb-2010-11-2-r14
73. Luo W, Brouwer C. Pathview: an R/Bioconductor package for pathway-based data integration and visualization. Bioinformatics. 2013;29(14):1830–1831. doi: 10.1093/bioinformatics/btt285
74. Fabregat A, Sidiropoulos K, Viteri G, et al. Reactome pathway analysis: a high-performance in-memory approach. BMC Bioinf. 2017;18(1):142. doi: 10.1186/s12859-017-1559-2
75. Ren X, Kuan PF. methylGSA: a Bioconductor package and shiny app for DNA methylation data length bias adjustment in gene set testing. Hancock j, editor. Bioinformatics. 2019;35(11):1958–1959. doi: 10.1093/bioinformatics/bty892
76. Yu G, He Q-Y. ReactomePA: an R/Bioconductor package for reactome pathway analysis and visualization. Mol Biosyst. 2016;12(2):477–479. doi: 10.1039/C5MB00663E
77. Dewey M. Metap: meta-analysis of significance values. 2021.
78. Laufer BI, Hwang H, Jianu JM, et al. Low-pass whole genome bisulfite sequencing of neonatal dried blood spots identifies a role for RUNX1 in down syndrome DNA methylation profiles. Hum Mol Genet. 2021;29(21):3465–3476. doi: 10.1093/hmg/ddaa218
79. Sheffield NC, Bock C. LOLA: enrichment analysis for genomic region sets and regulatory elements in R and Bioconductor. Bioinformatics. 2016;32(4):587–589. doi: 10.1093/bioinformatics/btv612
80. Ernst J, Kellis M. ChromHMM: automating chromatin-state discovery and characterization. Nat Methods. 2012;9(3):215–216. doi: 10.1038/nmeth.1906
81. Anastasiadi D, Esteve-Codina A, Piferrer F. Consistent inverse correlation between DNA methylation of the first intron and gene expression across tissues and species. Epigenet Chromatin. 2018;11(1):37. doi: 10.1186/s13072-018-0205-1
82. Liu X, Wang J, Sun G. Identification of key genes and pathways in renal cell carcinoma through expression profiling data. Kidney Blood Press Res. 2015;40(3):288–297. doi: 10.1159/000368504
83. Zhu M, Wang Z, Zhu Z, et al. Exploration of the mechanism of valsartan treatment in chronic renal failure: network pharmacology and experimental validation. J Clin Pharm Ther. 2023;2023(1):4837743. doi: 10.1155/2023/4837743

84. Qu W, Han C, Li M, et al. Revealing the underlying mechanism of diabetic nephropathy viewed by microarray analysis. Exp Clin Endocrinol Diabetes Off J Ger Soc Endocrinol Ger Diabetes Assoc. 2015;123(6):353–359. doi: 10.1055/s-0035-1548849
85. Li S, Xiao J, Huang C, et al. Identification and validation of oxidative stress and immune-related hub genes in Alzheimer's disease through bioinformatics analysis. Sci Rep. 2023;13:657. doi: 10.1038/s41598-023-27977-7
86. Becker K, Klein H, Simon E, et al. In-depth transcriptomic analysis of human retina reveals molecular mechanisms underlying diabetic retinopathy. Sci Rep. 2021;11(1):10494. doi: 10.1038/s41598-021-88698-3
87. Fang Z-Q, Zang W-D, Chen R, et al. Gene expression profile and enrichment pathways in different stages of bladder cancer. Genet Mol Res GMR. 2013;12(2):1479–1489. doi: 10.4238/2013.May.6.1
88. He Z, Tang F, Lu Z, et al. Analysis of differentially expressed genes, clinical value and biological pathways in prostate cancer. Am J Transl Res. 2018;10(5):1444–1456.
89. Ji X, Bossé Y, Landi MT, et al. Identification of susceptibility pathways for the role of chromosome 15q25.1 in modifying lung cancer risk. Nat Commun. 2018;9:3221. doi: 10.1038/s41467-018-05074-y
90. Yang Y, Huang Z, Yuan M, et al. Genomic and transcriptomic characterization of pre-operative chemotherapy response in patients with osteosarcoma. Sci Rep. 2023;13(1):20914. doi: 10.1038/s41598-023-46857-8
91. Owens DF, Kriegstein AR. Is there more to gaba than synaptic inhibition? Nat Rev Neurosci. 2002;3(9):715–727. doi: 10.1038/nrn919
92. Wildman SS, Dunn K, Van Beusecum JP, et al. A novel functional role for the classic CNS neurotransmitters, GABA, glycine, and glutamate, in the kidney: potent and opposing regulators of the renal vasculature. Am J Physiol Ren Physiol. 2023;325(1):F38–F49. doi: 10.1152/ajprenal.00425.2021
93. Yang Y, Ren L, Li W, et al. Gabaergic signaling as a potential therapeutic target in cancers. Biomed Pharmacother. 2023;161:114410. doi: 10.1016/j.biopha.2023.114410
94. Macdonald RL, Kang J-Q, Gallagher MJ. Mutations in GABAA receptor subunits associated with genetic epilepsies. J Physiol. 2010;588 (Pt 11):1861–1869.
95. Ramamoorthi K, Lin Y. The contribution of GABAergic dysfunction to neurodevelopmental disorders. Trends Mol Med. 2011;17 (8):452–462. doi: 10.1016/j.molmed.2011.03.003
96. Collins AL, Ma D, Whitehead PL, et al. Investigation of autism and GABA receptor subunit genes in multiple ethnic groups. Neurogenetics. 2006;7(3):167–174. doi: 10.1007/s10048-006-0045-1
97. Soltani N, Qiu H, Aleksic M, et al. GABA exerts protective and regenerative effects on islet beta cells and reverses diabetes. Proc Natl Acad Sci. 2011;108(28):11692–11697. doi: 10.1073/pnas.1102715108
98. Al-Kuraishy HM, Hussian NR, Al-Naimi MS, et al. The potential role of pancreatic γ-aminobutyric acid (GABA) in diabetes mellitus: a critical reappraisal. Int J Prev Med. 2021;12(1):19. doi: 10.4103/ijpvm.IJPVM_278_19
99. Wan Y, Wang Q, Prud'homme GJ. Gabaergic system in the endocrine pancreas: a new target for diabetes treatment. Diabetes Metab syndr obes targets Ther. Diabetes Metabolic Syndr Obes Targets Ther. 2015;8:79–87. doi: 10.2147/DMSO.S50642
100. Tian J, Lu Y, Zhang H, et al. γ-Aminobutyric acid inhibits T cell autoimmunity and the development of inflammatory responses in a mouse type 1 diabetes model. J Immunol. 2004;173 (8):5298–5304. doi: 10.4049/jimmunol.173.8.5298
101. Fairbrother-Browne A, Ali AT, Reynolds RH, et al. Mitochondrial-nuclear cross-talk in the human brain is modulated by cell type and perturbed in neurodegenerative disease. Commun Biol. 2021;4 (1):1–14. doi: 10.1038/s42003-021-02792-w
102. Sly WS, Hu PY. Human carbonic anhydrases and carbonic anhydrase deficiencies. Annu Rev Biochem. 1995;64(1):375–401. doi: 10.1146/annurev.bi.64.070195.002111
103. Mishra CB, Tiwari M, Supuran CT. Progress in the development of human carbonic anhydrase inhibitors and their pharmacological applications: where are we today? Med Res Rev. 2020;40 (6):2485–2565. doi: 10.1002/med.21713
104. Ciccone L, Cerri C, Nencetti S, et al. Carbonic anhydrase inhibitors and Epilepsy: state of the art and future perspectives. Molecules. 2021;26(21):6380. doi: 10.3390/molecules26216380
105. Pollard A, Shephard F, Freed J, et al. Mitochondrial proteomic profiling reveals increased carbonic anhydrase ii in aging and neurodegeneration. Aging (Albany NY). 2016;8(10):2425–2436. doi: 10.18632/aging.101064
106. Shah GN, Bonapace G, Hu PY, et al. Carbonic anhydrase ii deficiency syndrome (osteopetrosis with renal tubular acidosis and brain calcification): novel mutations in CA2 identified by direct sequencing expand the opportunity for genotype-phenotype correlation. Hum Mutat. 2004;24(3):272–272. doi: 10.1002/humu.9266
107. Bosley TM, Salih MA, Alorainy IA, et al. The neurology of carbonic anhydrase type ii deficiency syndrome. Brain. 2011;134 (12):3502–3515. doi: 10.1093/brain/awr302
108. Ma H-L, Yu S-J, Chen J, et al. CA8 promotes RCC proliferation and migration though its expression level is lower in tumor compared to adjacent normal tissue. Biomed Pharmacother. 2020;121:109578. doi: 10.1016/j.biopha.2019.109578
109. Türkmen S, Guo G, Garshasbi M, et al. CA8 mutations cause a novel syndrome characterized by ataxia and mild mental retardation with predisposition to quadrupedal gait. Barsh GS, editor. PLOS Genet. 2009;5(5):e1000487. doi: 10.1371/journal.pgen.1000487
110. Morita M, Imanaka T. Peroxisomal ABC transporters: structure, function and role in disease. Biochim Biophys Acta. 2012;1822 (9):1387–1396. doi: 10.1016/j.bbadis.2012.02.009
111. Pohl A, Devaux PF, Herrmann A. Function of prokaryotic and eukaryotic ABC proteins in lipid transport. Biochim Biophys Acta. 2005;1733(1):29–52. doi: 10.1016/j.bbalip.2004.12.007
112. Höftberger R, Kunze M, Weinhofer I, et al. Distribution and cellular localization of adrenoleukodystrophy protein in human tissues: implications for X-linked adrenoleukodystrophy. Neurobiol Dis. 2007;28(2):165–174. doi: 10.1016/j.nbd.2007.07.007
113. Tawbeh A, Gondcaille C, Trompier D, et al. Peroxisomal ABC transporters: an update. Int J Mol Sci. 2021;22(11):6093. doi: 10.3390/ijms22116093
114. Kemp S, Pujol A, Waterham HR, et al. ABCD1 mutations and the X-linked adrenoleukodystrophy mutation database: role in diagnosis and clinical correlations. Hum Mutat. 2001;18(6):499–515. doi: 10.1002/humu.1227
115. Sun X, St John JC. Modulation of mitochondrial DNA copy number in a model of glioblastoma induces changes to DNA methylation and gene expression of the nuclear genome in tumours. Epigenet Chromatin. 2018;11(1):53. doi: 10.1186/s13072-018-0223-z
116. Lopes A. Mitochondrial metabolism and DNA methylation: a review of the interaction between two genomes. Clin Epigenet. 2020;12 (1):182. doi: 10.1186/s13148-020-00976-5
117. Pogribny IP, James SJ, Beland FA. Molecular alterations in hepatocarcinogenesis induced by dietary methyl deficiency. Mol Nutr Food Res. 2012;56(1):116–125. doi: 10.1002/mnfr.201100524
118. Aon MA, Cortassa S, Juhaszova M, et al. Mitochondrial health, the epigenome and healthspan. Clin Sci Lond Engl 1979. 2016;130 (15):1285–1305. doi: 10.1042/CS20160002
119. Minocherhomji S, Tollefsbol TO, Singh KK. Mitochondrial regulation of epigenetics and its role in human diseases. Epigenetics. 2012;7 (4):326–334. doi: 10.4161/epi.19547
120. Hong YS, Battle SL, Puiu D, et al. Long-term air pollution exposure and mitochondrial DNA copy number: an analysis of UK Biobank data. Environ Health Perspect. 2023;131(5):057703. doi: 10.1289/EHP11946
121. Solomon WL, Hector SBE, Raghubeer S, et al. Genome-wide DNA methylation and LncRNA-Associated DNA methylation in metformin-treated and -untreated diabetes. Epigenomes. 2020;4 (3):19. doi: 10.3390/epigenomes4030019
122. Lozoya OA, Martinez-Reyes I, Wang T, et al. Mitochondrial nicotinamide adenine dinucleotide reduced (NADH) oxidation links the tricarboxylic acid (TCA) cycle with methionine metabolism and

nuclear DNA methylation. PLOS Biol. 2018;16(4):e2005707. doi: 10.1371/journal.pbio.2005707
123. Zeisel SH. Choline, other methyl-donors and epigenetics. Nutrients. 2017;9(5):445. doi: 10.3390/nu9050445
124. Kottakis F, Nicolay BN, Roumane A, et al. LKB1 loss links serine metabolism to DNA methylation and tumourigenesis. Nature. 2016;539(7629):390–395. doi: 10.1038/nature20132
125. Kaufman BA, Durisic N, Mativetsky JM, et al. The mitochondrial transcription factor TFAM coordinates the assembly of multiple DNA molecules into nucleoid-like structures. Mol Biol Cell. 2007;18(9):3225–3236. doi: 10.1091/mbc.e07-05-0404
126. Filograna R, Mennuni M, Alsina D, et al. Mitochondrial DNA copy number in human disease: the more the better? FEBS Lett. 2021;595(8):976–1002. doi: 10.1002/1873-3468.14021
127. Rusecka J, Kaliszewska M, Bartnik E, et al. Nuclear genes involved in mitochondrial diseases caused by instability of mitochondrial DNA. J Appl Genet. 2018;59(1):43–57. doi: 10.1007/s13353-017-0424-3
128. Lee SR, Han J. Mitochondrial nucleoid: shield and switch of the mitochondrial genome. Oxid Med Cell Longev. 2017;2017(1):8060949. doi: 10.1155/2017/8060949
129. Mei H, Sun S, Bai Y, et al. Reduced mtDNA copy number increases the sensitivity of tumor cells to chemotherapeutic drugs. Cell Death Dis. 2015;6(4):e1710. doi: 10.1038/cddis.2015.78
130. Aasumets K, Basikhina Y, Pohjoismäki JL, et al. TFAM knockdown-triggered mtDNA-nucleoid aggregation and a decrease in mtDNA copy number induce the reorganization of nucleoid populations and mitochondria-associated ER-membrane contacts. Biochem Biophys Rep. 2021;28:101142. doi: 10.1016/j.bbrep.2021.101142
131. Kremer LS, Gao G, Rigoni G, et al. Tissue-specific responses to TFAM and mtDNA copy number manipulation in prematurely ageing mice. Gurkar au, Kapahi P, editors. Elife. 2025;14:RP104461. doi: 10.7554/eLife.104461.3
132. Westermann L, Li Y, Göcmen B, et al. Wildtype heterogeneity contributes to clonal variability in genome edited cells. Sci Rep. 2022;12:18211. doi: 10.1038/s41598-022-22885-8
133. Santos GC, Zeidler JD, Pérez-Valencia JA, et al. Metabolomic analysis reveals vitamin D-induced decrease in Polyol pathway and subtle modulation of glycolysis in HEK293T cells. Sci Rep. 2017;7(1):9510. doi: 10.1038/s41598-017-10006-9
134. Wang Y, Yang D, Wang M. Signaling profiles in HEK 293T cells co-expressing GLP-1 and gip receptors. Acta Pharmacol Sin. 2022;43(6):1453–1460. doi: 10.1038/s41401-021-00758-6
135. Chen Z, Huang Y, Chen Y, et al. CircFNDC3B regulates osteoarthritis and oxidative stress by targeting miR-525-5p/HO-1 axis. Commun Biol. 2023;6(1):200. doi: 10.1038/s42003-023-04569-9